technische universität
dortmund

**Arbeit zur Erlangung des akademischen Grades
Master of Science**

Alignment studies for the LHCb SciFi Detector

Nils Breer
geboren in Unna

2022

Lehrstuhl für Experimentelle Physik V
Fakultät Physik
Technische Universität Dortmund

Erstgutachter: Prof. Dr. Albrecht
Zweitgutachter: Dr. Weingarten
Abgabedatum: May 16th 2022

Abstract

Due to larger luminosities and higher track multiplicity, detectors with finer granularity are needed. The LHCb experiment is undergoing a major upgrade during the long shutdown of the LHCb between 2019 and 2022. The three tracking detectors downstream of the dipole magnets are undergoing a replacement with a detector that consists of scintillating fibers (SciFi). The calibration of the new detector to the software regarding orientation and position is critical for the subsequent performance. This process is called *alignment* and is part of the trigger and is a crucial part of the real-time analysis of the LHCb.

In this work, the software *alignment* of the SciFi tracker is studied. So called *misalignment* tests contributed to determine the quality of the alignment. In addition, tests for the identification of weak modes were performed. This drew attention to a bias within the SciFi hit clusters which was observed to have an impact on the performance of the alignment procedure.

Kurzfassung

Aufgrund größerer Luminositäten und höherer Spurmultiplizitäten werden Detektoren mit feinerer Granularität benötigt. Das LHCb-Experiment wird während der langen Abschaltung des LHCb zwischen 2019 und 2022 einem größeren Umbau unterzogen. Die drei Spurdetektoren hinter den Dipolmagneten werden durch einen Detektor ersetzt, der aus szintillierenden Fasern (SciFi) besteht. Die Kalibrierung des neuen Detektors mit der Software hinsichtlich Ausrichtung und Position ist entscheidend für die spätere Leistung. Dieser Prozess wird *alignment* genannt und ist Teil des Triggers und ein entscheidender Teil der Echtzeitanalyse des LHCb.

In dieser Arbeit wird das Software-*Alignment* des SciFi-Trackers studiert. Sogenannte *misalignment*-Tests trugen zur Bestimmung der Qualität des Alignments. Darüber hinaus wurden Tests zur Identifizierung von schwachen Moden durchgeführt. Dies machte auf einen Bias innerhalb der Cluster aufmerksam welcher einen nicht-unwichtigen Einfluss auf das Alignment hat.

Inhaltsverzeichnis

1 Introduction

At the beginning of the 20th century many physicists started research on elementary particles and the interactions associated with them. The combined knowledge lead to the construction of one of the most precisely tested theories: the Standard Model (SM) of particle physics. Flavor anomalies show strong tensions with Standard Model and also the recent publication on the W-boson mass measurement is challenging the accuracy of the Standard Model[10]. No single measurement or anomaly on its own is enough to be in a total disagreement with the SM, but combined they provide hints that the SM is not the final theory. The SM describes every fundamental force except for gravity. There are still open questions such the baryon asymmetry of the universe requiring a, by several orders of magnitude, larger charge-parity (CP) violation than the SM predicted. To tackle these problems, high energy experiments such as the Large Hadron Collider beauty (LHCb) experiment located at the Large Hadron Collider (LHC) at CERN were built for this exact reason. The LHCb experiment was designed to study beauty and charm quarks with focus on measuring CP-violation and searching for New Physics in rare decays. To detect these phenomena, the threshold for statistical uncertainties has to be lowered and the amount of data collected needs to be increased. The upgrade described in section 2.3.2 allows us to have a five times higher instantaneous luminosity of $2 \cdot 10^{33}$ 1/fb with the expected detector readout rate of 40 MHz. To realize these hardware and software challenges, the front-end electronics, tracking systems and the trigger system needed upgrades. To operate the upgraded LHCb at its full potential, it is of great importance that all detector components are brought into an alignment level so that the impact on physical observables is insignificant.

The Alignment theory will be described in chapter 3. In chapter 4 different sets of constraints, degrees of freedom and alignable objects called *configuration* will be tested first in order to study how different configurations influence the alignment. Afterwards several tests will be performed to analyse the behavior of a misaligned detector and check if the chosen configuration converges towards an aligned state. The deviations from a centered state after the alignment are needed for other trigger stages to be known in the reconstruction. The LHC will not run permanently at maximum luminosity therefore tests are performed to analyse alignment of different luminosity samples. Especially while the LHC restarts it will run at a lower luminosity. During the alignment studies a bias inside the Scintillating Fibre hit

clustering algorithms was discovered which had an impact on the alignment. The exact changes will be discussed in the final section of chapter 4.

2 Particles and The Large Hadron Collider

With good alignment, studies on all Standard Model (SM) particles and hadron states will improve. Yielding better efficiencies on SM particle measurements will result in deeper insights regarding physics beyond the Standard Model from high-precision measurements of CP-violating observables as an example.

On a grand scheme upgrading the LHCb and therefore the LHC will bring deeper insights on Standard Model processes. This will help us to understand the universe even better and eventually yield information about the unsolved question of "dark matter" and "dark energy", what is believed to be the bulk of the universe's content.

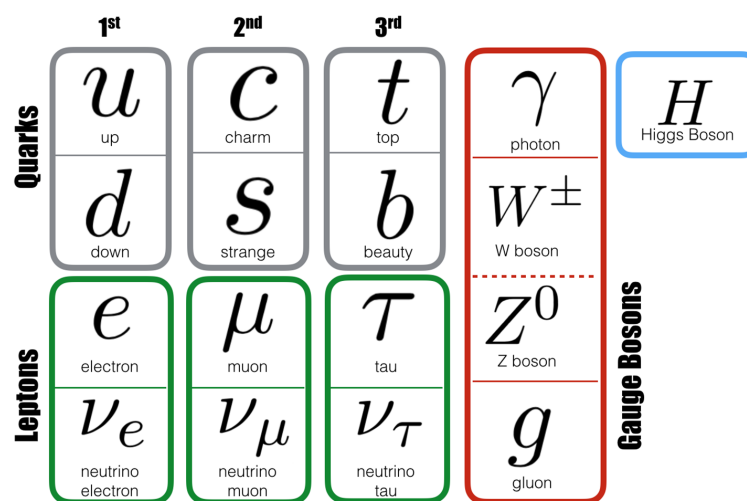## 2.1 The Standard Model

Abbildung 2.1: The Standard Model of particle physics[21].

The Standard Model of particle physics describes the known elementary particles and their interactions. It consists of 12 matter particles, the fermions and five interaction particles. which are called gauge bosons.

The fermions consists of 12 spin-1/2 particles. Six are called leptons and they are sorted into three families, also called flavors (e, μ and τ) and six are called quarks. Each of those lepton families has a charged lepton[1] and a left-handed neutrino. A particle has a left-handed helicity if its spin direction is opposite to the direction of flight. Right-handed helicity particles have a spin direction pointing with the direction of flight. Neutrinos can only be left-handed since there is no system where the neutrino can be "overtaken" so the momentum switches and therefore the helicity. The leptons can couple via the weak-interaction and if they are charged, also via the electromagnetic (em) interaction. Neutrinos can only couple via the weak interaction. Each matter particle also has an anti particle, with an opposite quantum numbers.

The quarks carry an electric charge as well. In each of the three generations there is one isospin doublet. In the first generation are the two lightest quarks, up- and down quark, in the second generation the charm- and strange quark and in the third generation the top- and bottom quark doublet. Quarks carry a colour charge (anti quarks carry the respective anti-colour), red, green or blue, which is an artificially introduced degree of freedom to guarantee the distinguishability. The summary of all particles is shown in figure 2.1.

The interactions are mediated through the gauge bosons. The three interactions are the EM-interaction, the weak interaction and the strong interaction. Gravitation does not make a significant contribution. The gauge boson of the EM-interaction is the photon which is exchanged between particles.

The strength of each interactions is described by a coupling constant. In the EM interaction this is the fine structure constant[18]. The range of the EM-interaction is in principle infinite, but decreases with increasing distance between the interacting particles. The EM-interaction is described by quantum electrodynamics (QED). The potentials are described by operators, which create and annihilate the photons.

The exchange particles of the weak interaction are on the one hand the $W^{\pm}$-bosons and on the other hand the Z-boson. The weak interaction processes are called currents. Changing the charge during the interaction by a W-boson is called charged current. The exchange reaction of a Z boson in, for example, processes such as $e_{\nu}\mu \rightarrow e_{\nu}\mu$ is called neutral current. Analogous to the EM-interaction, the potentials are again understood as operators, but here there are no propagators. Propagators are used in *Feynman*-diagrams of QED to represent the interaction particles. A so-called V-A structure is used here instead. Here, V stands for vectorboson and A is the axialvector. This structure is needed to disregard the right-handed particles and left-handed antiparticles, since these lead to the charge-parity violation. Thus

---

[1]can have both handnesses

the Lorentz factors are adjusted in the following way

$$\gamma_\mu \rightarrow \gamma_\mu (1 - \gamma_5)$$

Quarks couple via the strong interaction which is described by quantum chromodynamics (QCD). The Lie group of the QCD is $SU(N = 3)$ where N is the number of introduced colors as a new degree of freedom. The number of generators is therefore $N^2 - 1 = 8$. The generators are called gluons and they carry color and anticolor, have no mass and carry spin 1. Gluons can, other than photons, couple to themselves. Moreover, the coupling constant is $\alpha_s \approx 0.1$.

The second wavefunction describes a gluon interaction with a blue quark and changing the color to red. Quarks thus tend to attract each other very strongly. If now quark and anti quark are moved away from each other, a lot of energy has to be expended. This energy can become so large that new particles can be created. Quarks and gluons also have a property called confinement, which means that coloured states cannot exist alone." Instead they form bound states, so called hadrons. On the one hand there are the mesons, which consist of a quark and an antiquark.

These may be from the same family (i.e. [u,d], [c,s], [t,b]), or from different families. Mesons have a baryon number of 0. Accordingly, quarks carry the baryon number $\frac{1}{3}$. The quarks constructing a meson therefore carries color and the corresponding anticolor. The second type are baryons. The content consists of either three quarks or three antiquarks. However, it cannot be that one quark and two antiquarks and vice versa occur, because baryons must have the baryon number B = 1.

2.2 Particle decays and hadrons

The LHCb experiment is especially designed for *b*- and *c*-hadrons because of the forward production, which is shown in figure 2.4. Measurements in the heavy quark flavour sector have shown observations of $B_s^0 \rightarrow \mu^+\mu^-$ [2] as well as measurements of the flavour changing neutral current (FCNC) anomaly in the $B^0 \rightarrow \phi\mu^+\mu-$. The former one is a very rare leptonic decay and is CKM suppressed but it is sensitive to new physics. New physics can be in penguin decays which are forbidden at tree level in the SM. The latter is possible via penguin decays with very small branching fractions[4]. The LHCb group also measured the B_s^0 mass difference[3] Δm_s through the oscillation frequency in $B_s^0 \rightarrow D_s^\mp \pi^\pm$ decays.

2.3 The LHC and LHCb

2.3.1 The LHC

The Large Hadron Collider (LHC)[14] is the largest particle-accelerator on planet earth. With a circumference of 26.7km it is also the longest ring accelerator and it lies between 45m and 170m below the surface near Geneva in Switzerland. The tunnel was constructed for the Large Electron-Poitron Collider (LEP) between 1984 and 1989 and was replaced by the LHC, operated by the European Organization for Nuclear Research (CERN). The LHC can collide at centre-of-mass energies of $\sqrt{s} = 13\,\text{TeV}$ in proton-proton collisions during Run 2. The design centre-of-mass energy after the upgrade is $\sqrt{s} = 14\,\text{TeV}$.[8] An image of the accelerators and the experiments is shown in figure 2.2.
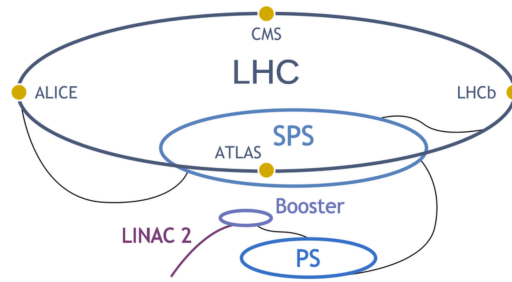

Abbildung 2.2: An overview of the LHC facilities[1]. The full description is in the main part of this thesis.

By ionizing hydrogen gas, protons are created and accelerated to $50\,\text{MeV}$ by the linear accelerator (LINAC 2). Afterwards the beam is injected into the Proton Synchrotron (PS) and the Super Proton Synchrotron (SPS) to a maximum of $450\,\text{GeV}$ before the beam is injected into the LHC. The beam consists of several bunches with around $1{,}15 \cdot 10^{11}$ protons per bunch and a bunch spacing of $25\,\text{ns}$.The LHC houses four major experiments. ATLAS and CMS are classified as general purpose detectors

with a detection range of close to 4π. The interaction in these detectors is located in the very center so that tracks going in every direction can be reconstructed.These detectors were built for the search for the Higgs Boson, but are used for many other physics studies. The other two Experiments located at the LHC are ALICE and LHCb. The ALICE experiment mainly studies the quark-gluon plasma during the runs with lead ion collisions instead of protons.
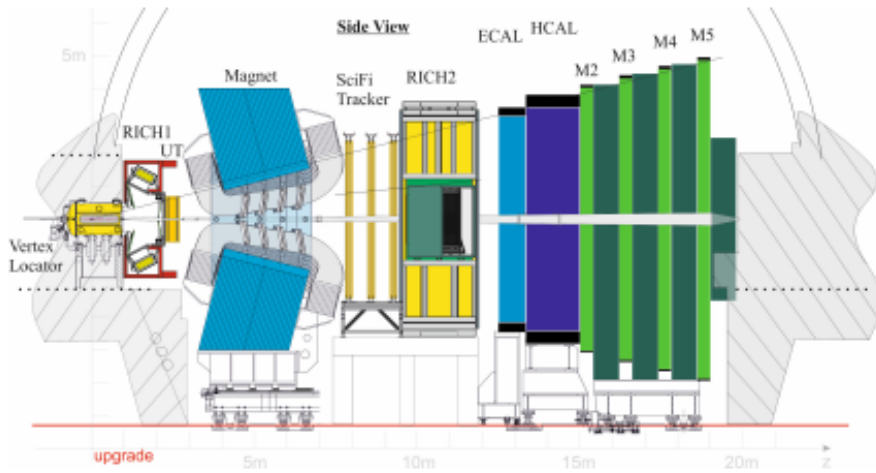
2.3.2 The LHCb experiment

Abbildung 2.3: A side view of the upgraded LHCb experiment[19].

For high energies, b- and $\bar{b}$-quarks are abundantly boosted into a relatively narrow cone depending on the exact energy, as seen in figure 2.4[2] with a production cross section of $144 \pm 1 \pm 21\mu b$ [5] for $13\,TeV$ from previous measurements. The uncertainties are statistical and systematic, respectively. The LHCb experiment[23] is a forward spectrometer covering $2 < \eta < 5$ in the pseudorapidity range and due to the production angles of heavy flavour it is beneficial to have the geometry as it is. Unfortunately financial resources prevent building a symmetrical detector covering negative η. The main physics goal of the LHCb experiment is in the beauty- and charm-quark sector. A side-view of the new LHCb is shown in figure 2.3.

The Vertex Locator (VELO) is the tracking detector dedicated to primary vertex precision measurements as well as tracking displaced vertices of particles with short lifetimes, which are most of the reasonable particles. The upgraded tracking layers

---

[2]They are also produced in backward direction but the experiment is only build for the forward cone.

use $50 \times 50\mu m^2$ pixels for a finer hit resolution as well as a better track reconstruction. The previous VELO was $8.4\,mm$ away from the beam pipe. The new VELO will be $5.1\,mm$ away from the beam pipe so that the particles enter the detector earlier and interact with less detector material before the first interaction layer is hit. This will improve the impact parameter resolution as well as the tracking resolution of the VELO for tracks with low momentum[20]. The Upstream Tracker (UT) will be utilized for better momentum resolution, ghost suppression and is a necessity for Downstream tracking. The UT is a necessary component for the improvement of the trigger timing and it also contributes to the improvement of momentum resolution. The UT consists of 4 tracking layers using silicon strips. Analogous to the VELO the inner sensors will be closer to the beam axis in comparison to the current tracker. Due to the expected radiation dose and particle distribution throughout the tracker, the out region uses a p^+-in-n technology for the strips and the strips in the middle region uses n^+-in-p technology to better withstand the higher radiation. The strips closest to the beam use n^+-in-p technology as well. The Scintillating Fibre Tracker (SciFi) is located downstream of the magnet region. Therefore measurements regarding particle momentum can be provided.A detailed description is presented in section 2.4. Close to the interaction point (IP) the Ring Imaging Cherenkov counter (RICH1) is located. Its purpose is p, π and K particle identification (PID). The upgraded RICH1 will be able to handle the increasing particle occupancy dude to the increase of the focal length by a factor of $\sqrt{2}$. The readout rate will be increased from currently $1\,MHz$ to $40\,MHz$, realized by Multianode Photomultipliers (PMTs). The hadronic calorimeter and electromagnetic calorimeter as well as the four muon chambers are used for p, e, γ and μ PID. The front-end electronics of the calorimeters are being replaced during the upgrade.

In this section, a general overview about the requirements for the SciFi Tracker as well as the layout will be described based on the presentation in the *technical design report*[15] of the upgrade.

The upstream and downstream trackers provide a good precision estimate of the momentum of charged particles so that mass resolutions of decayed particles can be precisely measured. For particle identification the reconstructed trajectories of charged particles are used as input for the RICH detectors. The limiting factor for the momentum resolution is multiple scattering for tracks with a momentum lower than $80\frac{GeV}{c}$. For tracks with a higher momentum the detector resolution is the limiting factor.

The Scintillating Fibre (SciFi) Tracker replaced the Inner Tracker (IT) and the Outer Tracker (OT) and is located in the same place as the downstream trackers that were previously installed.
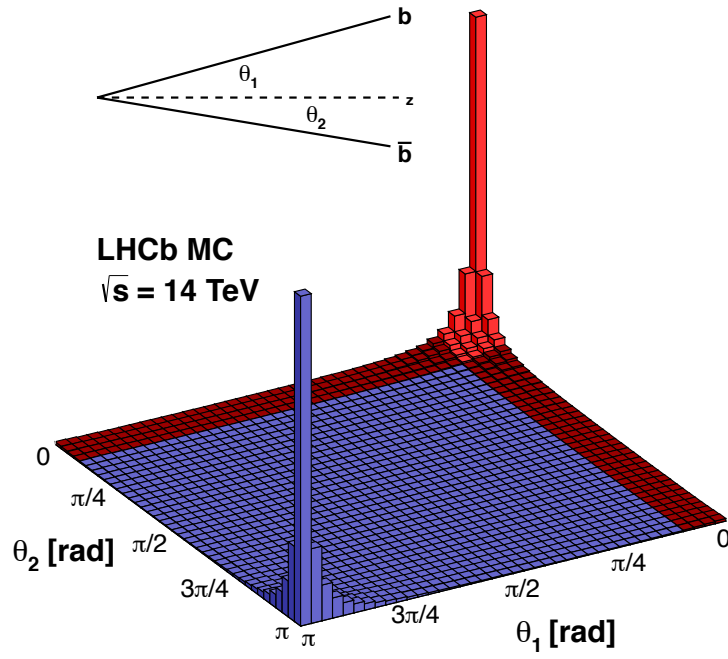
Abbildung 2.4: b-$\bar{b}$ forward production in the LHCb experiment[12].

The instantaneous luminosity after the upgrade is expected to be $1\,1/(\text{cm}^2\,\text{s})$ bis $2 \cdot 10^{33}\,1/(\text{cm}^2\,\text{s})$ with a bunch spacing of $25\,\text{ns}$. The average number of proton-proton interactions per bunch crossing will be between $\nu = 3.8$ and $\nu = 7.6$ during the startup and the latter is the estimate for the upgrade MC.

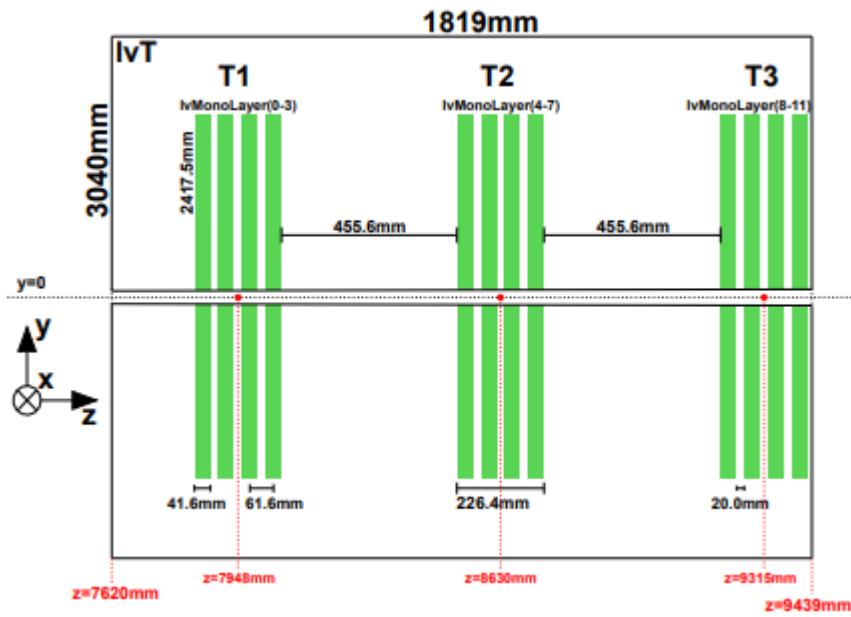## 2.4 The SciFi Tracker

2.4.1 Layout of the SciFi Tracker

Abbildung 2.5: Side view of the SciFi geometry. The beam pipe lies in the horizontal slot between the upper and the lower half of the figure.[15]

The SciFi Tracker consists of three stations T1, T2 and T3 each having four layers $(X1, U, V, X2)$. The orientation of these planes with respect to the vertical axis are $(0°, 5°, -5°, 0°)$. Since the beampipe is not exactly parallel to the ground the vertical axis is defined as vertical on the z-axis of the beampipe. The tilted layers are called stereo layers and serve the purpose of 3D hit localization. A visualization of the stereo angle is shown in figure 2.6. The layers are $20\,\text{mm}$ apart from each other in z-direction within each station. Each layer in the first two stations has four quarters with each quarter having five modules, with the layers in station three having six modules. Each module is constructed from four fibre mats. A frontal view of the SciFi Tracker is displayed in figure 2.5. The global coordinate system
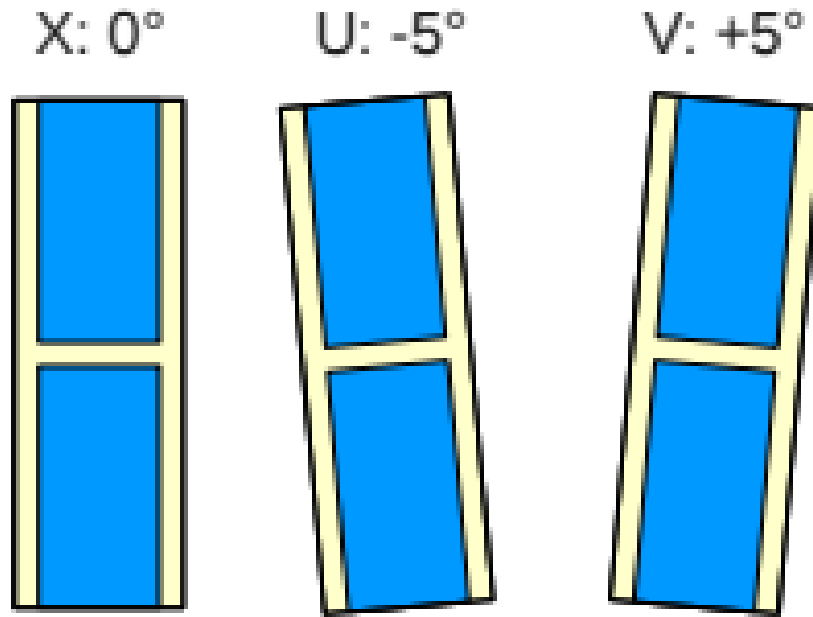
Abbildung 2.6: Visualization of the stereo angles of the U- and V-layer with respect to the X-layers.

used is of right-handed nature with positive z pointing away from the interaction point following the beam direction as seen in figure 2.3. positive y points upwards, towards the surface and positive x and negative x are named as A-Side and C-Side respectively[15]. For readout purposes the top and bottom half of each element have inverted x- and y-axis as seen in figure 2.5.

To ensure an optimal alignment, a well known geometry is key. Therefore, the fibres within each mat must be aligned within $50\,\mu m$ bis $100\,\mu m$ in x-direction and must not be more than $300\,\mu m$ bent in z-direction.

2.4.2 Scintillating Fibres

The scintillating fibre material is a polymer with an organic fluorescent dye added to the polystyrene structure to enhance the yield during the scintillation process. In order to produce and register a photon signal, the ionization energy is deposited in the fibre core. The amount of energy need for the polymer to reach an excited state is just a few electronvolts[25]. The added dye has the particular structure to match the excitation energy. The dye generates excited energy states when particles hit the fibre and deposit their energy. The refractive index difference between the core

of the fibre and the outer cladding make sure total internal reflection occurs, which guides the photons to the silicon photomultipliers (SiPMs). On the opposite end of the mat a full reflective mirror is mounted so the photons travelling to the other end do not get lost but reflected towards the SiPM. The amount of light reaching the SiPMs is reduced by the radiation damage of the fibres.

3 The Theory of Alignment

Whenever a new detector is built, people are careful to mount it as close to the correct location as they can. In order to check this, survey measurements are performed to check the position with a precision of 100 μm. To achieve an even greater precision, *software alignment* is performed.

The reason why alignment is of great importance is that a misaligned detector yields worse momentum resolutions, low reconstruction efficiencies and biased mass estimations and mass peak resolutions. The most prominent area of misalignment for a spectrometer are asymmetries. In the past, alignment solved problems for example a Muon asymmetry in the L0Muon trigger in 2011 and a misalignment in IT boxes which resulted in trigger inefficency regarding J/Ψ in 2012.

3.1 Clustering of SciFi hits

The signals generated by the SiPMs are read out by a specifically developed integrated circuit, the *PACIFIC*[1][17]. It performs the shaping, integration and digitization of the signal. An effect called spillover caused by the propagation delay of photons inside the fibres and the recovery time of the SiPMs. This leads to the signal not being completely inside of its 25-ns timeslot for the bunch crossing. The *PACIFIC* shapes the signal from the SiPM to reduce the spillover and suppress the signal tails[9]. Afterwards, the signal is integrated over the 25-ns timeslot and a 2-bit analog-digital converter (ADC) digitizes the signal. Three comparators implement the ADC and can be set individually for each channel, as seen in figure 3.1.

To achieve a reduction in data rate and suppress the signal noise, clusterization is performed. A diagram of the clusterization is shown in Figure 3.2

During the digitization the specific thresholds are set. The second comparator sets the *seeding threshold* which marks channels exceeding said threshold as cluster candidates. Up to three more neighboring channels can be added to the cluster if they pass the threshold set by the first comparator (*neighboring threshold*). The third comparator sets the *high threshold*. A cluster can be form by just one channel if it

---
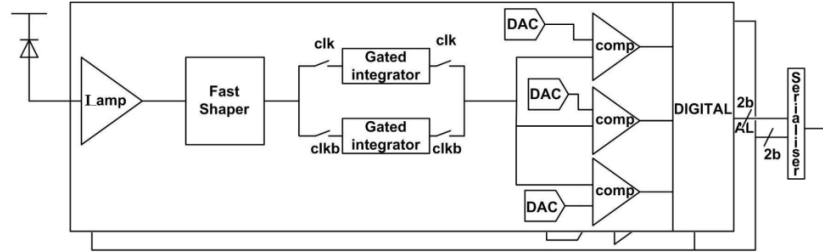
[1](low Power Asic for the sCIntillating Fibres traCker

Abbildung 3.1: Figure of the PACIFIC chip. From left to right, an amplifier, a shaper and an integrator are build in. The Signal the is digitized and the Clustering is performed to the 2-bit output on the far right.
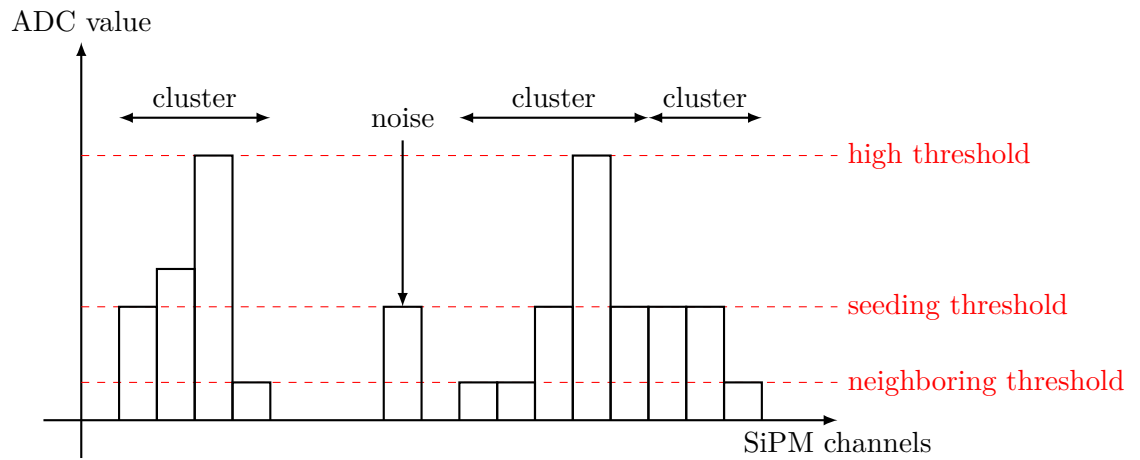

Abbildung 3.2: Clusters are created by a group of channels from which one must be above the seeding threshold and the other channels being above the neighboring threshold. The other option is for one cluster being above the high threshold. Cluster with a width larger than four channels.

exceeds this threshold. The cluster position is the weighted mean of the contributing channels to this cluster. The cluster resolution can be better than $100\,\mu m$ [9]. In the next section, the way that clusters are combined to reconstruct tracks is described.

3.2 Track Reconstruction

In order for LHCb to be used for physics, all of the detector hit information has to be converted into tracks, which is a challenging task. The track reconstruction algorithm needs to find the correct hits from each sub detector to build the track. This can be problematic just because of the amount of tracks per event (roughly 100). The aim is to have the track efficiency as high as possible. in order to estimate the track parameters, such as the curvature parameter and track slopes (t_x, t_y), as accurately as possible. A good track fit is needed in order to find to best estimates for the track parameters and covariances. The estimates are used in the event reconstruction to find the correct tracks for each particle and the decay products. The information provided is used in the RICH rings, ECAL and HCAL and muon detectors. With these information, particle and track parameters such as the invariant mass can be measured and vertex origins of particle decays can be found. There are several track models that can be used. In general, a track is built from numerous segments which are either straight or curved because of an active magnetic field. Depending on the environment of the track either model is good. The track segments are called track states and are defined by a position in x and y at a given distance z where the hit was located, then a slopes $t_{x,y}$ at the hit position and a momentum parameter obtained from the track curvature inside the magnetic field[24].

In order to correctly reconstruct the track it is important to know where the hit is localized and for the upcoming hits, where to particle track came from. From the momentum measurement of the track curvature caused by the magnetic field, the parameter q/p is also added where q stands for the charge of the track that is determined from the direction into which of the track bends.

$$\vec{r} = \begin{pmatrix} x \\ y \\ t_x \\ t_y \\ \frac{q}{p} \end{pmatrix} \qquad t_x = \frac{\partial x}{\partial z} \qquad\qquad t_y = \frac{\partial y}{\partial z}$$

The uncertainty of the five-component state vector is a 5×5 covariance matrix C. A track state can be anywhere on the trajectory but is easier to choose it at real

detection points. Combining the track state with a real measurement point is called *node*. The propagation from node $k-1$ to node k is described by a propagation function

$$\vec{r}_k = f_k(\vec{r}_{k_{-1}}) + \vec{w}_k \, .$$

This means node k is acquired by propagating node $k-1$ through the propagation function f_k and shifting it by the *process noise* $\vec{w}_k$.

LHCb uses process noise to model the scattering caused by particle interactions with the detector material. Depending on the type of propagation, linear or curved, a different propagation function is used. for a linear extrapolation, f_k results in

$$f_k(\vec{r}_{k-1}) = F_k \vec{r}_{k-1}$$

with the transport matrix F_k

$$F_K = \begin{pmatrix} 1 & 0 & \Delta z & 0 & 0 \\ 0 & 1 & 0 & \Delta z & 0 \\ 0 & 0 & 1 & 0 & 0 \\ 0 & 0 & 0 & 1 & 0 \\ 0 & 0 & 0 & 0 & 1 \end{pmatrix}$$

and Δz being the difference in z between the nodes

$$\Delta z = z_k - z_{k-1}$$

Trajectory information for each node is provided by the real measurement where the relation between measurement m_k and track state at a given node k is defined as

$$m_k = h_k(\vec{r}_k) + \epsilon_k$$

with the projection function h_k and *measurement noise* ϵ_k. So if the detector only measures the y coordinate of state, the projection function will be

$$h_k(\vec{r}_k) = H_k \vec{r}_k$$

with

$$H_k = \begin{pmatrix} 0 & 1 & 0 & 0 & 0 \end{pmatrix} \, .$$

When measuring more parameters the measurement matrix H_k and projection matrix have dimension $n \times 5$ with n being the numbers of parameters measured.

With this track model, ϵ_k and w_k are random and unknown and have an expectation value of zero.

3.3 The Kalman filter method

In general a track is an ensemble of measurements and track states and the Kalman filter method[24] is used to fit tracks. The idea of the Kalman filter is, to have a starting node and add measurements one by one. In between the addition of measurements, the local track state is updated with the new information. The Kalman filter method is a χ^2 minimising problem for the measurement of the track. Because of the iterative nature of the method, it is fast and also used in other fields than physics, for example GPS and meteorology. The three steps of the Kalman filter will be briefly outlined and later described in further detail.

The first step is the ***Prediction***: The next track state of the trajectory is predicted based on the track state at the previous node. The second step is the ***Filter*** procedure: By using filter equations, the prediction is updated with measurement information in this node. The prediction and filter are repeated for each measurement. With more measurements added, the estimate for the best trajectory is the track state after each filter step. The final step is called ***Smoother***: When the trajectory is complete, smoother equations are applied from the last node to the previous node. Therefore the information from all measurements is used in both forward- and back-propagation which results in a more defined track.

3.3.1 First Step: Prediction

For a given state vector at node *k-1*, the prediction for the kth state vector and its covariance matrix results from the propagation relations

$$\vec{r}_p^{k-1} = f_p\left(\vec{r}_{k-1}\right)$$
$$\text{Cov}_k^{k-1} = F_k C_{k-1} F_k^T + Q_k$$

The superscript of the state vector shows the amount of information used in the estimate. That means $\vec{r}_k^n$ is the smoothed state vector which used all information, $\vec{r}_k^k - 1$ is the predicted state vector and $\vec{r}_k^k \equiv \vec{r}_k$ is the filtered state.

Q_k is the process noise in matrix form and it is part of the predicted covariance matrix C_k^{k-1}. Because the first state cannot take measurements from the previous state, an initial prediction is taken from the track finding algorithm instead. The predicted residual between the measurement, m_k and the state vector results in

$$\text{res}_k^{k-1} = m_k - h_k\left(\vec{r}_k^{k-1}\right)$$

and the corresponding covariance matrix is defined as

$$\mathrm{Cov}_{\mathrm{res},k}^{k-1} = V_k + H_k C_k^{k-1} H_k^T \,.$$

Here, V_k is the measurement variance. With these metrics the minimal χ^2 for the optimal track states can be calculated via

$$\left(\chi^2\right)_k^{k-1} = \mathrm{res}_k^{k-1} \left(\mathrm{Cov}_{\mathrm{res},k}^{k-1}\right)^{-1} \mathrm{res}_k^{k-1}$$

3.3.2 second Step: Filter

During the filter step, the track state is updated with the measurement information. Iteratively, each measurement is added and the filtered state $\vec{r}_k$ and the corresponding covariance matrix is calculated via

$$\vec{r}_k = \vec{r}_k^{k-1} + G_p \mathrm{res} + k^{k-1}$$
$$\mathrm{Cov}_k = \left(\mathbb{1} - G_k H_k\right) \mathrm{Cov}_k^{k-1} \,,$$

where G_k is the gain matrix of dimension 5×1 and is defined as

$$G_k = C_k^{k-1} H_k^T \left(\mathrm{Cov}_{\mathrm{res},k}^{k-1}\right)^{-1}$$

Afterwards the residuals and its covariance matrix are calculated and the filtered total χ^2 is defined as

$$\left(\chi^2_{\mathrm{filter}}\right)_k = \mathrm{res}_k \mathrm{Cov}_{\mathrm{res},k}^{-1} \mathrm{res}_k \,.$$

The prediction and filter procedure is continued for all measurements until the track is fully reconstructed. Because the last node at $k = n$ has the most information in it, a backward update is performed to infuse the previous nodes with the same information as in last node. This is called *smoother*-step.

3.3.3 third Step: Smoother

The smoother function returns the best possible estimate for track states at the previous nodes. The method used is called *Rauch-Tung-Striebel*-smoother[22]. The idea is to use backward information and construct a smoothed state vector and covariance matrix

$$\tilde{r}_k^n = \vec{r}_k + S_k \left(\vec{r}_{k+1}^n - \vec{r}_{k+1}^k\right)$$
$$\tilde{C}_k^n = C_k$$

and the Smoother-matrix S_k of dimension 5×5

$$S_k = C_k F_{k+1}^T \left(C_{k+1}^p\right)^{-1} .$$

In order to calculate the smoothed χ^2 the residual and corresponding covariance matrix are

$$\text{res}_k = m_k - h_k \vec{h}_k^n$$
$$\text{Cov}_{\text{res},k}^n = V_k - H_k C_k^n H_k^T$$

The χ^2 is calculated analogously to the one during the filter step with the difference being the new residuals and covariances.

3.4 Alignment with Kalman filter track fit

In principle, minimizing the track residuals is the obvious way to align a detector. The residual $\vec{\text{res}}_k$ is defined by the difference between a real detector hit and the expected hit position

$$\text{res}_k = m_k - h_k(\vec{r}, \vec{\alpha}) \tag{3.1}$$

where $\boldsymbol{h}$ is the measurement model, $\vec{r}$ are the track parameters and $\vec{\alpha}$ are the alignment parameters. Aligning the SciFi by minimizing the track χ^2 with the same model as used for reconstruction is an advantage. The idea is to use a global covariance matrix in the track fit with the kalman filter. This approach will be used as the type of alignment for the SciFi in this thesis. In the following paragraph this form of alignment is briefly described[13].

Because of the similarity to the kalman filter method a short revisit of the minimum χ^2 formalism is presented. The track χ^2 is defined as

$$\chi^2 = \vec{\text{res}}^T V^{-1} \vec{\text{res}} , \tag{3.2}$$

where V is the track covariance matrix. Equation (3.2) is a matrix expression since m and h are vectors and V a symmetric matrix. For a linear expansion of the measurement model for an initial estimate x_0 of the track parameters.

$$h(x) = h(x_0) + H(x - x_0)$$

with H, the projection matrix, being defined as

$$H = \frac{\partial h(x)}{\partial x}|_{x_0} .$$

The minimal χ^2 condition with respect to x can be written as

$$\frac{\mathrm{d}\chi^2}{\mathrm{d}x} = 0 = -2H^T V{-}1 \left(m - h(x_0) - H(x - x_0) \right) .$$

The solution to this equation is the known expression of the least-square estimator defined as

$$x = x_0 - CH^T V^{-1} \left(m - h(x_0) \right) \tag{3.3}$$

with C being the covariance matrix regarding x.

$$C = \left(H^T V^{-1} H \right)^{-1} \tag{3.4}$$

The non-linear case for the measurement model (x dependency of H) the solution in equation (3.3) is of iterative nature and can be applied until convergence is achieved. That can be the minimum change in χ^2 for which the first and second derivative are needed so the change in the current estimate x_0 is defined as

$$x - x_0 = - \left(\frac{\mathrm{d}^2\chi^2}{\mathrm{d}x^2}|_{x_0} \right)^{-1} \frac{\mathrm{d}\chi^2}{\mathrm{d}x}|_{x_0} .$$

Expanding the model by alignment parameters α. The condition for χ^2 to be minimal with respect to a track model $h(x, \alpha)$ with track parameters x_k and alignment parameters α_k are

$$\frac{\partial \sum_k \chi_k^2}{\partial \alpha} = 0 \tag{3.5}$$

and

$$\forall_k \frac{\partial \chi_k^2}{\partial x_k} = 0 . \tag{3.6}$$

The subscript j denotes the track not the vector component. For a single track the subscript can be left out. The more number of tracks, the more number of parameters in the minimizing problem. For a large number of tracks a similar expression as in equation (3.3) for the least squares estimator is used and the computation is performed in two steps since the inverse matrix is computationally too expensive to use a least squares expression. The first step is to estimate track parameters for a starting set of calibration parameters called α_0. The second step is to minimize the total χ^2 with respect to α while also taking x_j and α into account.

The total derivative reads

$$\frac{\mathrm{d}}{\mathrm{d}\alpha} = \frac{\partial}{\partial\alpha} + \frac{\mathrm{d}x}{\mathrm{d}\alpha}\frac{\partial}{\partial x}\,. \tag{3.7}$$

$\frac{\mathrm{d}x}{\mathrm{d}\alpha}$ is a derivative matrix and results from the minimal track χ^2 condition and can be expressed by

$$\frac{\mathrm{d}}{\mathrm{d}\alpha}\frac{\partial\chi^2}{\partial x} = 0 \tag{3.8}$$

therefore the derivative matrix is defined as

$$\frac{\mathrm{d}x}{\mathrm{d}\alpha} = -\frac{\partial^2\chi^2}{\partial\alpha\partial x}\left(\frac{\partial^2\chi^2}{\partial x^2}\right)^{-1}\,. \tag{3.9}$$

The total χ^2 for a sample of tracks is minimal with respect to α and x can the be described as

$$\frac{\mathrm{d}\chi^2}{\mathrm{d}\alpha} = 0\,. \tag{3.10}$$

For N alignment parameters a system with N coupled non-linear equations is defined. Linearizing the minimum χ^2 condition around the starting values α_0 and solving the linear system for $\Delta\alpha$ yields the solution.

$$\frac{\mathrm{d}^2\chi^2}{\mathrm{d}\alpha^2}|_{\alpha_0}\Delta\alpha = -\frac{\mathrm{d}\chi^2}{\mathrm{d}\alpha}|_{\alpha_0} \tag{3.11}$$

Now, with enough constraints inside the alignment the second derivative matrix is invertable and the covariance matrix for α reads

$$\mathrm{Cov}(\alpha) = 2\left(\frac{\mathrm{d}^2\chi^2}{\mathrm{d}\alpha^2}\right)^{-1}\,.$$

Higher order derivatives in α are neglected here. The difference in the total χ^2 resulting from a change in $\Delta\alpha$ is given by

$$\Delta_{\chi^2} = \frac{1}{2} \left(\frac{\mathrm{d}\chi^2}{\mathrm{d}\alpha} \right)^T \Delta\alpha = -\Delta\alpha^T \mathrm{Cov}(\alpha)^{-1} \Delta\alpha$$

The change in total χ^2 is equivalent to the significance of the alignment correction and Δ_{χ^2} is used to follow the convergence of an alignment.

4 Alignment of the SciFi

For the upgrade the LHCb detector was completely rebuilt. In place of the previous IT and OT a new tracking detector was built which utilizes scintillating fibre called SciFi Tracker. The front-end electronics were also upgraded to handle the increasing data rate. For the new SciFi Tracker a new software is used.

Because of the introduction of the new software, the alignment configuration needs to be determined from the beginning. The goal is to find a configuration that can accurately reproduce the position of the real detector and can correct for "weak modes". With some alignment parameters being highly correlated, detector components may move in the same direction or by the same amount. This is called a "weak mode". The movements do not affect the alignment χ^2 since the residuals have not changed. Results of weak modes are biases in track parameters and poor alignment convergence. One of the most visible weak modes is the curvature bias. There a different ways to reduce the effect of weak modes for example using an overlapping detector design or using different data sets to gather more information.

4.1 Alignment Configuration

An alignment configuration is a specific selection of detector elements, alignment parameters, constraints and track- and vertex-selections used for the alignment. Alignment parameters are the specific degrees of freedom used for the alignment and for each detector element. The Alignment parameters can be any combination of translations and rotations around the x, y and z axis(Tx, Ty, Tz, Rx, Ry, Rz). The configuration that produces the best estimate for the detector position is the best candidate and will be used for the Run 3 data taking. A track and vertex reconstruction is performed before the alignment is evaluated. Depending on the tracks used the output can be different. Mainly two different track selections will be used throughout the thesis shown in table 4.1

The alignment runs were performed with alignment specific packages from Alignment/Escher and Alignment/TAlignment[6]. During the alignment, Lagrange constraints can be utilized to minimize alignment parameter α under the condition

$$f(\alpha) = 0 \tag{4.1}$$

Tracks	Selections
GoodLongTracks	$P_{\text{total, min}} = 5000\,\text{MeV}$
	$P_{\text{total, max}} = 200\,000\,\text{MeV}$
	$p_{\text{T, min}} = 200\,\text{MeV}$
	maximum $\chi^2 = 5$
	"long" track type
HighMomentumTTracks	$P_{\text{total, min}} = 50\,000\,\text{MeV}$
	maximum $\chi^2 = 5$
	"TTrack" track type

Tabelle 4.1: SciFi track selection.

and adding the Lagrange parameter λ to get

$$\Delta\chi^2 = \lambda f(\alpha)\,. \tag{4.2}$$

Lagrange constraints are added to fix loosely constrained degrees of freedom and can be used for any linear combination of translations and rotations as shown in table 4.2

Tx, Ty, Tz	translation in x, y, z
Rx, Ry, Rz	rotation around x, y, z
Szx, Szy	shearing of x and y along z
Szz, Sxx	scaling in x and z

Tabelle 4.2: Lagrange constraints that can be used as alignment parameters.

An illustration of shearing is shown in figure 4.1.

In the software, a Langrange constraint is defined by three elements. A name which can be chosen by the user, the detector element and the alignment parameters, seperated by a colon.

The starting constraints are defined as the following table 4.3, which are based on the alignment conditions from the OT and knowledge from experts.

The SciFi Tracker is referred to as Forward Tracker (FT) in the software. The first element in each row of the starting conditions is the detector element. The first set of six numbers are hardcoded parameters for each of the three translation degrees of freedom and three rotational degrees of freedom (Tx, Ty, Tz, Rx, Ry, Rz). They are set to be zero to match the known position of the detector in the Monte Carlo Simulation (MC). and the second set of six parameters are the corresponding
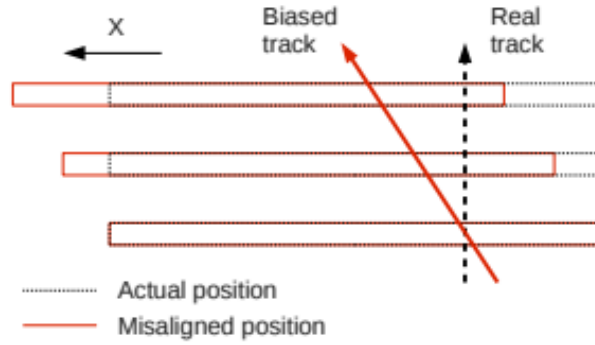
Abbildung 4.1: An illustration of shearing.

element	positions	uncertainties
FT	0 0 0 0 0 0	1 1 1 0.0003 0.0003 0.0003
FT/T.	0 0 0 0 0 0	1 1 1 0.0003 0.0003 0.0003
FT/T./Layer(X1|U|V|X2)	0 0 0 0 0 0	0.2 0.2 0.2 0.0001 0.0001 0.0001
FT/.*Module.	0 0 0 0 0 0	0.1 0.1 0.1 0.001 0.001 0.001
FT/.*Mat.	0 0 0 0 0 0	0.05 0.05 0.05 0.1 0.1 0.1

Tabelle 4.3: starting condition of the SciFi Tracker.

uncertainties. The scale for the translations are mm and the scale for the rotations being rad. A survey uncertainty of 0,0001 stands for 0,1 mrad. During this thesis, the LHC beam was off and the SciFi detector was still being constructed. The alignment tests in this thesis use Monte Carlo simulated data to test the alignment software for the SciFi.

4.2 Null tests and software tests

4.2.1 Software configurations and samples

At first, a series of tests regarding different degrees of freedom and Lagrange constraints is performed to find the optimal solution for the SciFi Tracker.

The detector layers in the MC are all centered around the beam pipe with no shifting in any direction and the goal is to align the real detector layers to mirror the layers in the software and reduce the shifting as close to zero as possible.
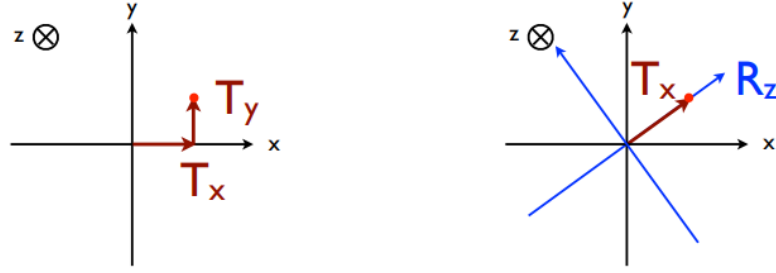
Abbildung 4.2: Different ways of describing a measurement point inside the detector(draw this again).

Figure 4.2 is used to demonstrate which degrees of freedom can be used to describe a point in the detector or a shift in coordinates. On the left-hand side the measurement point is described through cartesian coordinates and on the right-hand side it is described via polar coordinates.

Problems with the shearing constraints were seen in the VELO alignment, so that a similar analysis for the SciFi was considered. The parameters used for the VELO were changed to fit the SciFi Tracker and resulted in the following configuration:

```
dofs = "TxTzRxRz"
elements.FTStations(dofs)
elements.FTFrameLayers(dofs)
TrackSelections = GoodLongTracks()
```

The dataset[1] used taken from the TestFileDB[16] and will be used for the upcoming tests until a different set is mentioned. As the DoFs, x- and z-translation as well as rotations around the x- and z-axis are used and are the only relevant DoFs for the alignment since y-translation and rotations around the y-axis can be constructed from the other degrees of freedom. For the alignment runs, ten iterations were used and is not using input misalignment, so a perfectly aligned detector is expected from the MC. The alignment constants after each iteration are passed on to the next iteration. Convergence of the alignment is defined by the difference between the variation of the alignment parameters of the current iteration to the last iteration. If the variation is sufficiently small, the alignment is converged. The alignable objects are the (T-)stations and the frame layers within a station and the track selection is chosen to be *GoodLongTracks* as a starting point. This will be called *baseline* or *baseline configuration*. The baseline is unconstrained in order to check the accuracy of the alignment software without constraints and look for weak modes. The baseline

---

[1]upgrade_DC19_01_MinBiasMU

is completely unconstrained. The frame layers, also called half layers, are divided into two quarters which are the top half and bottom half of the frame layer.

4.2.2 Aligning with translations and constraints

The first configuration tested against the baseline is called "noRotation". Comparisons of this configuration with the baseline are shown in figure 4.3 and figure 4.4, for 1000 and 7000 simulated events respectively.

In these plots, the measurement points are the mean position of each layer, and the errorbars are root-mean-square errors (RMS) and come from the difference between the C-side and the A-side of the detector layer and is not the measurement uncertainty. The group position is the global position of the stations and layers inside the LHCb experiment, where $z = 0$ is the far left side of the experiment where the VELO begins.

The "noRotation" configuration is defined as:

```
dofs = "TxTz"
elements.FTStations(dofs)
elements.FTFramelayers(dofs)
TrackSelections = GoodLongTracks()
constraints = [
    "station1 : FT/T1 : Tx Tz",
    "station2 : FT/T2 : Tx Tz",
    "station3 : FT/T3 : Tx Tz",
    "frontCSide : FT/T3/Layer(X1|U)/Quarter(0|2) : Tx Tz",
    "backCSide  : FT/T3/Layer(V|X2)/Quarter(0|2) : Tx Tz",
    "frontASide : FT/T3/Layer(X1|U)/Quarter(1|3) : Tx Tz",
    "backASide  : FT/T3/Layer(V|X2)/Quarter(1|3) : Tx Tz"
]
```

The first three constraints on all stations regarding translations brings the movement of the frame layers within a station to around zero which can be seen clearly in figure4.3. The last four constraints restrict the sum of the movement of the half-layers inside each C-frame to be zero, which brings the x translation of the half-layers in station three even closer to zero. Even though the alignment improved the amount of constraints cannot recover from potential misalignments because the constraints hinder the stations from moving.

In an ideal alignment we want as few constraints as possible so that the alignable objects can be aligned and converge towards the optimal position based on the

track reconstruction. This measurement only used 1000 events and is only used as a guideline to what the trend of the distribution looks like. The associated graphs for Tx plotted against the group position in z are shown in figure 4.3.

A prominent problem visible is the layer separation between the X-layers and the stereo layers as well as a separation between the C-frames inside each station.
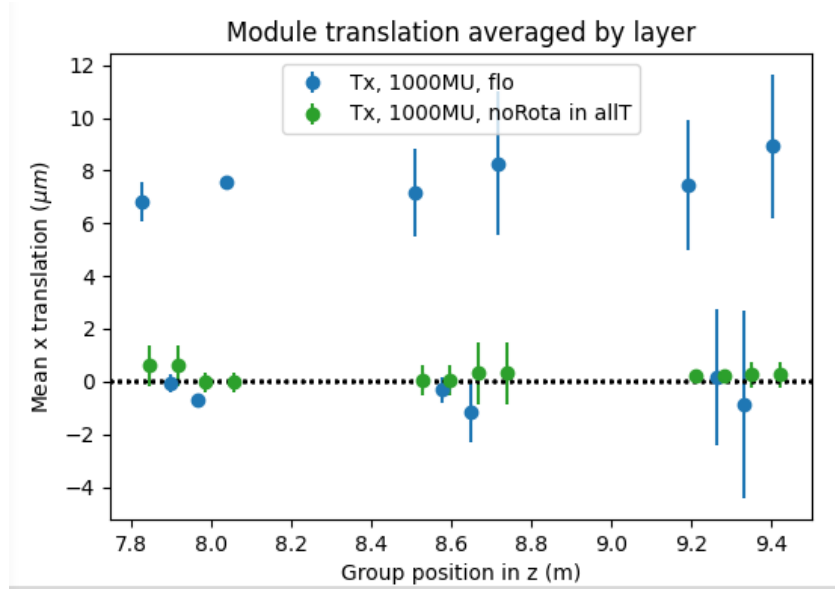

Abbildung 4.3: comparison of different configurations without rotational constraints in every station, magnet up and 1000 events. plotted is translation in x versus global z.

In figure 4.4 the same measurement was performed for 7000 events to get a better picture. In comparison to 4.3 an overall improvement of the baseline is visible and the layer-splitting is reduced but still prominent. The green measurement shows no direct improvement since the layers are already pretty close to zero in x-direction. Using 7000 events instead of 1000 events showed a more realistic picture but took more time to compute especially for 10 alignment iterations. For the following configuration, 3000 simulated events were used to shorten the computing time while still yielding an accurate representation of the situation.

4.2.3 Aligning with translations, rotations, and constraints

The next configuration tested will be called "half C-frame". This configuration is defined as
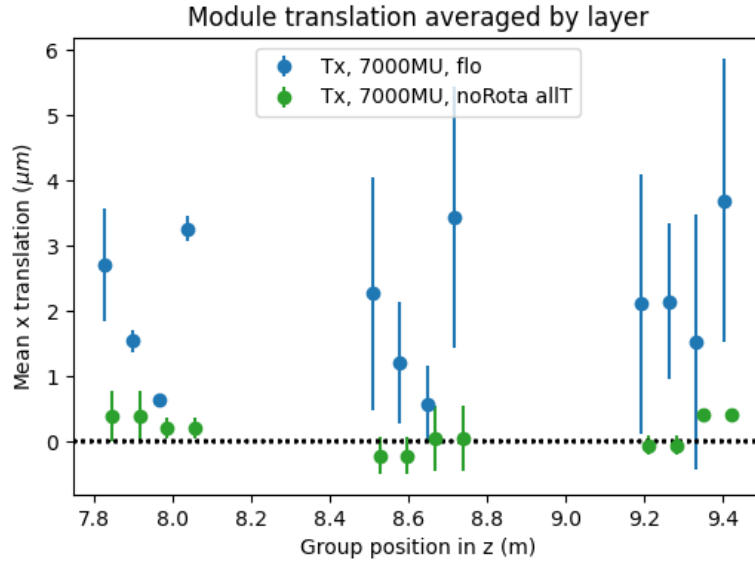
Abbildung 4.4: comparison of different configurations without rotational constraints in all stations, magnet up and 7000 events. plotted is x translation versus global z.

```
dofs = "TxTzRxRz"
elements.FTStations(dofs)
elements.FTFramelayers(dofs)
TrackSelections = GoodLongTracks()
constraints = [
    "station1 : FT/T1 : Tx Tz",
    "station2 : FT/T2 : Tx Tz",
    "station3 : FT/T3 : Tx Tz",
    "frontCSide : FT/T3/Layer(X1|U)/Quarter(0|2) : Tx Tz : total",
    "backCSide  : FT/T3/Layer(V|X2)/Quarter(0|2) : Tx Tz : total"
]
```

The degrees of freedom used for this configuration are the same as in the baseline configuration for the same reason. We chose to align the stations in the given DoFs to fix their overall position in the SciFi and also align the half-layers since we see a separation between the layers which we want to correct with the following constraints. The stations are constrained in Tx and Tz to fix the overall movement inside the SciFi. The second to last constraint ("frontCSide´´) is constraining the first to half-layers in station three in their total movement along the x- and z-axis. The last constraint works the same but for the back two half-layers of station three.

and the comparison to the baseline is shown in figure 4.5. Here the stations and layers are aligned in Tx, Tz, Rx and Rz but the stations are still only constrained in their translations. Also, the last station only has one side of each C-frame constrained. The additional keyword **total** constraints the difference of the quarters to zero with respect to the nominal position. As seen in figure 4.5 the first two layers have an average position of zero but the individual position is not. The same is seen in the last two layers of each station.

This new configuration in orange converged after 12 iterations as seen in figure 4.6. This figure shows the mean of the modules in each station per iteration. The modules of station one are the (colour1) dots, the modules for station two are coloured (colour2) and for station three is coloured (colour3). The horizontal red line is the nominal position of the SciFi in MC, where the aligned detector should be. The blue, dotted, vertical line marks the point of convergence for the alignment run. Normally, an alignment job should converge after three to five iterations. If the convergence happens later there could be a problem with the constraints which prevent the alignment from converging because they are implemented wrongly, are redundant or weak modes hinder the convergence.
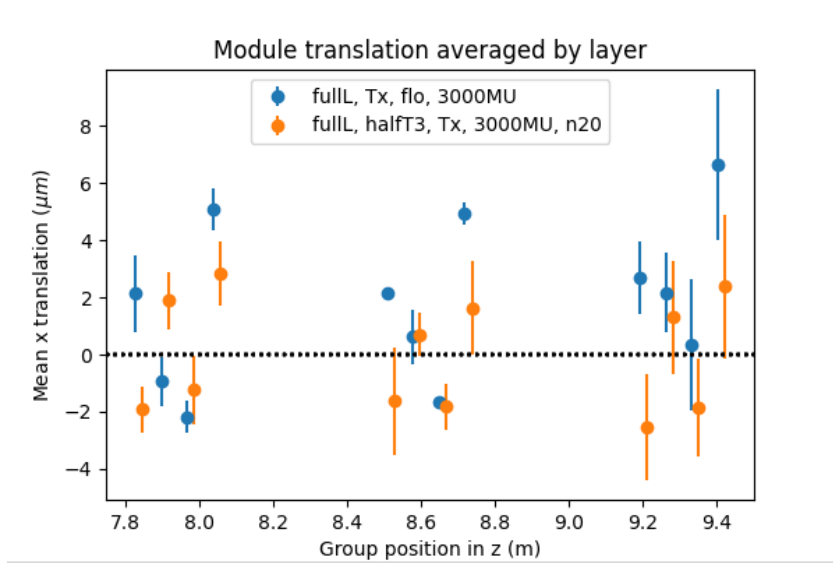
Abbildung 4.5: analysed 20 iterations for x translation behavior for configuration "half C-frame".
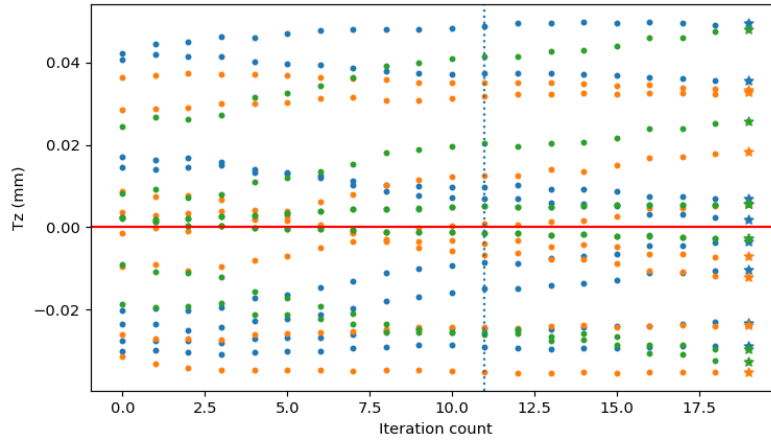
Abbildung 4.6: convergence of the alignment after 12 iterations from configuration "half C-frame".

4.3 rotational constraints

In the previous section rotations were not used inside the constraints. Now the constraints will include rotational constraints and test the changes.

Similar to the "noRotation" configuration the same constraints were used but for different degrees of freedom. The new configuration is called "Full DoF" which uses every degree of freedom and is defined as:

```
dofs = "TxTyTzRxRyRz"
elements.FTStations(dofs)
elements.FTFramelayers(dofs)
TrackSelections = GoodLongTracks()
constraints = [
    "station1 : FT/T1 : Tx Ty Tz Rx Ry Rz",
    "station2 : FT/T2 : Tx Ty Tz Rx Ry Rz",
    "station3 : FT/T3 : Tx Ty Tz Rx Ry Rz",
    "frontCSide : FT/T3/Layer(X1|U)/Quarter(0|2) : Tx Ty Tz Rx Ry Rz",
    "backCSide  : FT/T3/Layer(V|X2)/Quarter(0|2) : Tx Ty Tz Rx Ry Rz",
    "frontASide : FT/T3/Layer(X1|U)/Quarter(1|3) : Tx Ty Tz Rx Ry Rz",
    "backASide  : FT/T3/Layer(V|X2)/Quarter(1|3) : Tx Ty Tz Rx Ry Rz"
    ]
```

In figure 4.7 x-translation and z-translation with regards to the group position are shown.
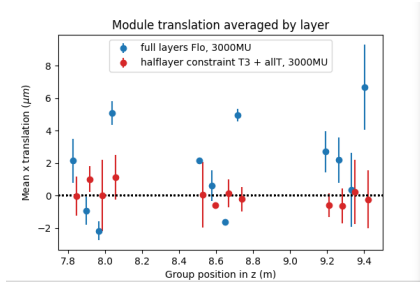
(a) x-translation versus group position in z.
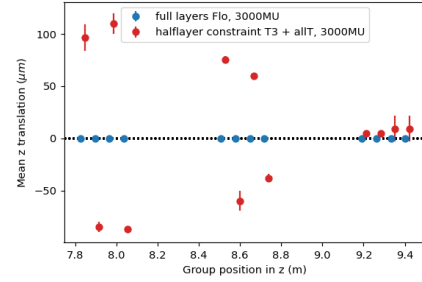
(b) z-translation versus group position in z.

Abbildung 4.7: "Full DoF" configuration (red) plotted versus baseline configuration (blue) for 3000 events.

Figure 4.7a still shows layer separation in station 1 more similar to figure 4.5 than to figure 4.4. Since the constraints are the same and the amount of degrees of freedoms increased, it is visible that using more DoFs makes the alignment worse. Therefore the degrees of freedom must be chose wisely.

Regarding the z-translation the plot is only shown to demonstrate the large separation of layers. the baseline was not aligned in Tz so there is no comparison.

The RMS uncertainty on the measurements is a result of the separation between A-side and C-side. For configuration "Full DoF", a plot showing the C-side and A-side difference in x-translation is shown in figure 4.8 and for z-translation in figure 4.9.

A clear layer separation is visible in terms af layer translation along the beam pipe4.8. The first and third layer in each station move away from the IP and the second and fourth layer move towards the IP. Because of the many constraints that are applied to T3, the RMS uncertainty in the other stations get worse. Because the last station is overconstrained the track reconstruction moves the other stations accordingly which results in a larger RMS uncertainty in station 1 and 2.

On the other hand the x-translation 4.9

Looking at figure 4.9, the last two layers in station 3 are seperated from the first two regarding x-translation. Especially the last station should be fixed around zero with the constraints added. The sum of all translations should be zero with each individual layer movement being small.

The result is unexpected with the constraints added and the cause of this problem is described later.
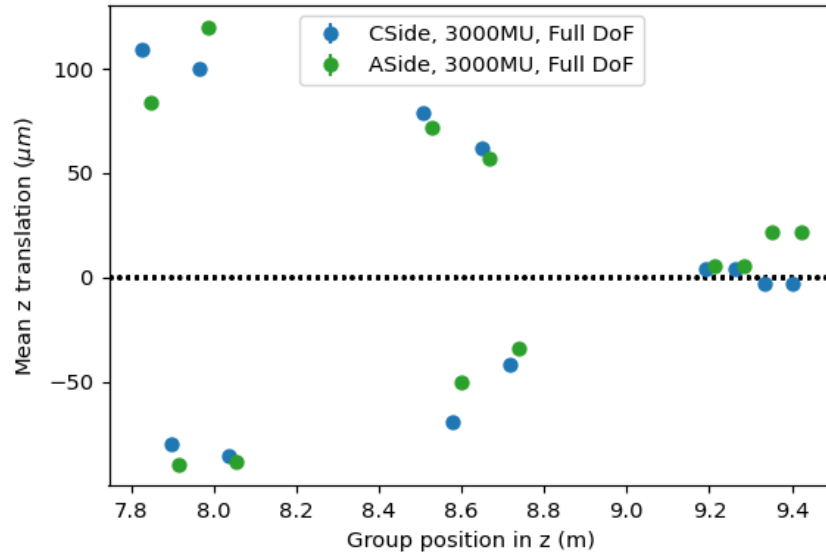
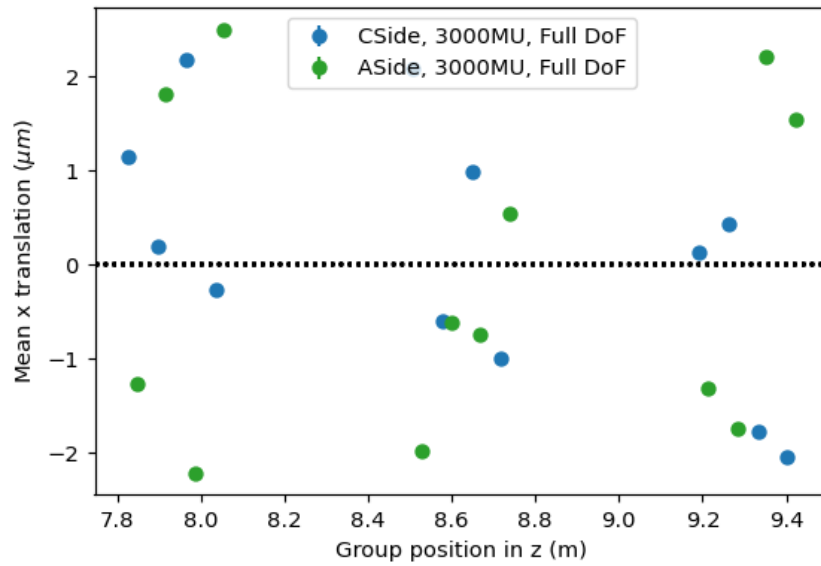**Abbildung 4.8:** compare C-Side to A-Side for translation in z direction.

**Abbildung 4.9:** compare C-Side to A-Side for translation in x direction.

4.3.1 Checking rotational degrees of freedom

The Next configuration tested is the result of a series of tests with various constraints, DoFs and alignable objects. In figure 4.10 a new configuration called "Test3" is introduced and it is defined as

```
dofs = "TxTzRxRz"
elements.FTStations(dofs)
elements.FTFramelayers(dofs)
TrackSelections = GoodLongTracks()
constraints = [
    "station3 : FT/T3 : Tx Tz Rx Rz",
    "frontCSide : FT/T3/Layer(X1|U)/Quarter(0|2) : Tx Tz Rx Rz",
    "backCSide  : FT/T3/Layer(V|X2)/Quarter(0|2) : Tx Tz Rx Rz",
    "frontASide : FT/T3/Layer(X1|U)/Quarter(1|3) : Tx Tz Rx Rz",
    "backASide  : FT/T3/Layer(V|X2)/Quarter(1|3) : Tx Tz Rx Rz"
    ]
```
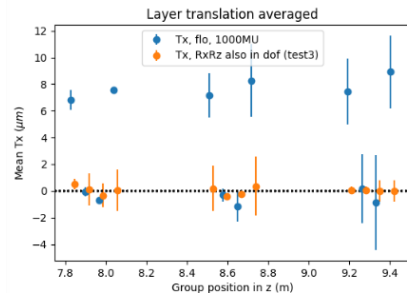

(a) x-translation versus group position in z.
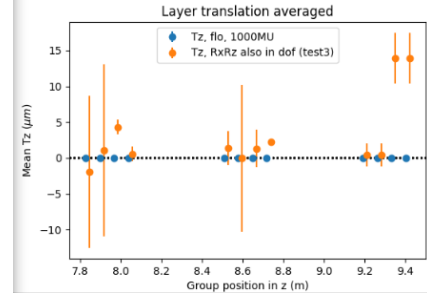
(b) z-translation versus group position in z.

Abbildung 4.10: "Test3" configuration (orange) plotted versus baseline configuration (blue) for 1000 events.

Here the last four C-frame constraints have rotational degrees of freedom added. Looking at 4.10a each station has a quite low movement in x-direction comparing to the previous configurations. In the last station, the first two layers the C-side and A-side are exactly where they should be inside the detector since the RMS is very close to zero. The last two layers only show a small uncertainty. In station two the X-layers are separating from the stereolayers. The X-layers also have a noticable RMS uncertainty. In this configuration the degrees of freedom are chose in a way for the alignment to either use them as two pairs of cartesian coordinates (Tx Tz, and Rx Rz) or interpret them as two pairs of polar coordinates (Tx Rz and Tz Rx). This and also the reduction in constraints seemed to help the alignment in terms

of x-translation, not so much regarding z-translation. Also this plot only shows the alignment for 1000 events and 10 iterations but overall an improvement was achieved when it comes to constructing a good configuration.

The next configurations are called "config5" (blue) and "config5 Rz" (orange). The plots showing the translations are shown in figure 4.11 and the rotations are shown in figure 4.12. The blue measurement has the same constraints as "Test3" with an added back C-frame constraint:

```
constraints.append("back_C_frame_T3 : FT/T3/Layer(V|X2) : Tx Tz")
```

The orange measurement has a similar constraint added with Rz added to the DoFs inside the constraint:

```
constraints.append("back_C_frame_T3 : FT/T3/Layer(V|X2) : Tx Tz Rz")
```

Comparing just these two configurations, regarding Tx there is not a big difference. The last station has a little more separation in "config5 Rz", station 2 shows roughly the same performance and station one is also more split, in total approximately 0,5 µm. The overall z-translation regressed by a small amount in every station while the layer speration in station 3 improved. It can be sen, that both X-layers in T2 in the x-translation plot have a quite large RMS uncertainty which means the A-side and the C-side in the X-layers are quite far apart but the mean is right around 0. That is expected since the constraint added only brings the mean of the layer to 0. In future analyses new constraints will be added to bring the sides together.
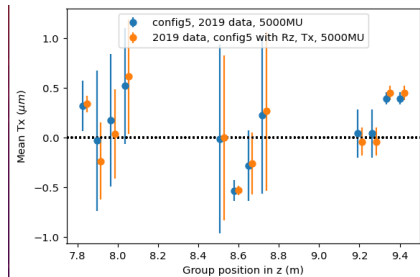
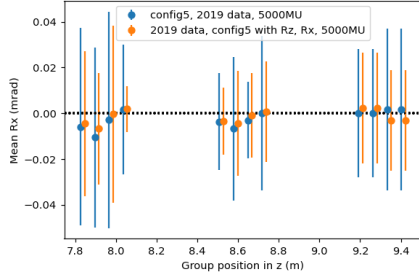(a) x-translation versus group position in z.
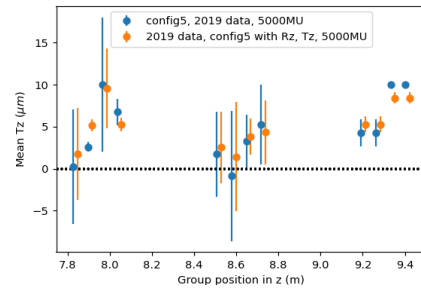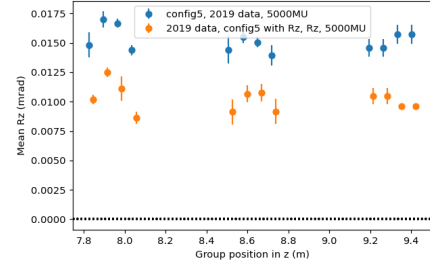

(b) z-translation versus group position in z.

Abbildung 4.11: "config5" configurations (blue) plotted versus "config5 Rz" configuration (orange) for 5000 events.

Rotations around x will not be further analysed because it does not have a huge impact on the alignment quality and is also very well aligned. In Rz a noticable gap between the two measurements can be seen. This is a result from the added

Rz constraint on the last two layers. The expected rotation is small than shown in figure 4.12b which is expected to be a result from bias in the clusters.

(a) x-rotation versus group position in z.

(b) z-rotation versus group position in z.

Abbildung 4.12: "config5" configurations (blue) plotted versus "config5 Rz" configuration (orange) for 5000 events.

Regarding the goal to reduce the amount of rotation and translation in each station, the result is a small improvement in *Rz* of around 0,005 mrad in every layer. *Rx* is mostly unchanged aswell as *Tx*.

Translation constraints as well as rotation constraints are not the only constraints tested. There are also scaling- and shearing constraints that were analysed but seemed to have no major impact.

4.4 chi2 tests and weak modes

In this section, a χ^2 analysis is performed in order to study the "goodness" of the alignment and determine the impact of potential weak modes also known as "correlated alignment parameters". There are several weak modes that could occur namely *global translation*, *shearing* and *curvature bias*. Weak modes are unaffected by the χ^2 since the residuals do not change but they do however show in terms of the eigenvalues of track parameters. The effect weak modes have on the alignment are biases regarding track parameters and late convergences. There are different solutions that can be utilized to reduce the effect from weak modes such as

- **using other data-taking configurations like magnet off or mass plots for off-axis eve**

- **utilizing other survey data sets**

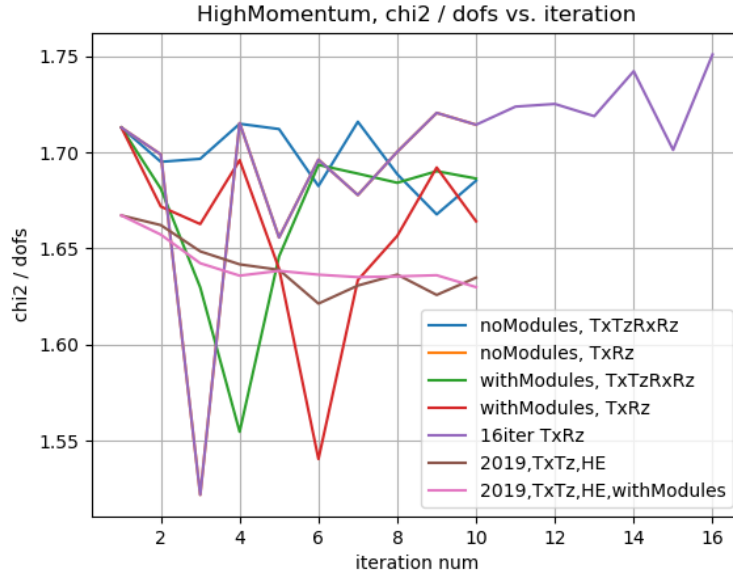- **using kinematic and vertex constraints**

Abbildung 4.13: $\chi^2/dofs$ versus iteration number of different degrees of freedom, alignables and data samples.

.

The first test is the χ^2-analysis for *HighMomentumTTracks*, 6500 events and 2020 data plotted versus the iteration number during the alignment in figure 4.13. In blue, stations and layers were aligned in Tx, Tz, Rx and Rz with the constraints being used from "config5". The orange measurement is identical except for the degrees of freedom being only Tx and Rz. In green and red the same measurements as in blue and orange were performed with the difference that that the modules are aligned as well. The purple measurement is the only one which covers 16 iterations and is otherwise identical to the orange one. That is also why the orange measurement is not visible since it lies behind the purple one for the first 10 iterations. the brown and pink measurements are done for 2019 data and are otherwise identical to the orange and red measurement regarding constraints and alignable degrees of freedom.

The spiky behavior in this plot is not what we expected and this might be the result of weak modes since the convergence is quite bad in all of the 2020 data which can be seen by the $\chi^2/dofs$ not steadily decreasing. The 2019 measurements were performed as control measurements with and without module alignment. Here a clear decrease in the $\chi^2/dofs$ is visible. This indicates that for the 2020 data additional analysis must be performed to gain further knowledge about the dataset

since it shows some unclear findings.

The idea to test Tx, Tz, Rx and Rz versus only one translation and one rotational degree of freedom was to analyse the effect regarding the convergence and the $\chi^2/dofs$ itself. One could also argue that there was a quick convergence after three iterations when looking at the yellow measurement but something happened afterwards. This will be analysed in a future project.

In figure 4.14 a comparison between GoodLongTracks and HighMomentumTTracks for the same measurements was performed to to study the impact of different track selections. This shows, that the alignment quality for both track selections increases with the number of iterations. The identical χ^2 measurements for the HighMomentumTTracks were plotted against the number of tracks as seen in figure 4.15 as an example. A clear correlation between the χ^2 dofs and the number of tracks can be seen.
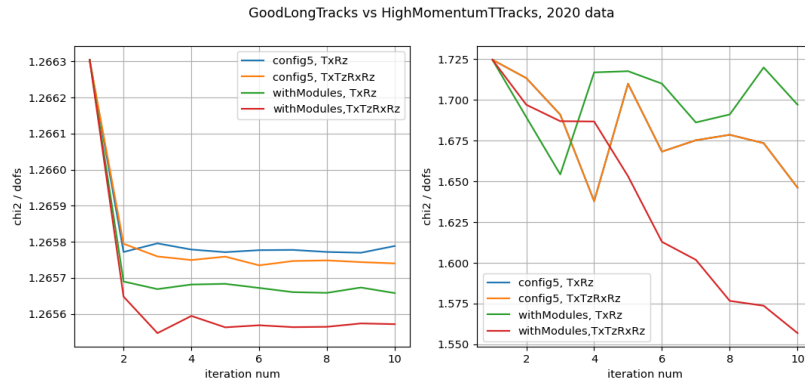

Abbildung 4.14: χ^2-test versus number of tracks of different degrees of freedom, alignables and data samples but fewer.

In figure 4.16 a side-by-side view of the same χ^2 measurement is shown but for different number of events. Despite the different labels these are the same measurements, only the colors are switched around for red and green and also yellow and blue as a pair. The thing that strikes the eye is the steadily decrease in $\chi^2/dofs$ in the red measurement. Unlike our first expectations that Tx and Rz are enough degrees of freedom to describe the system using additional degrees of freedom seemed to help the alignment. Also, the blue measurement sits behind the orange which might be due to an programming error.

In figure 4.17 a consistency check for figure 4.16 was performed. The number of tracks correlate well with the $\chi^2/dofs$. The blue measurement is missing again which seems to be a programming error.
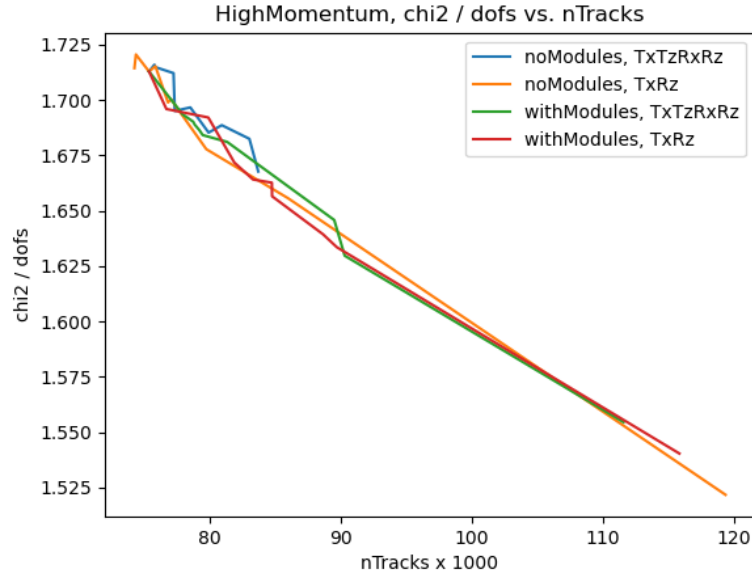
Abbildung 4.15: χ^2-test versus number of tracks of different degrees of freedom, alignables and data samples but fewer (redo with grid).
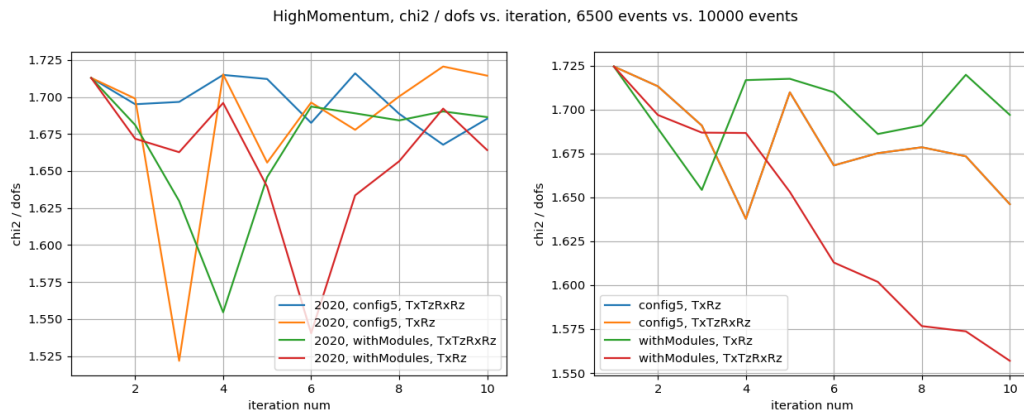

Abbildung 4.16: $\chi^2/dofs$ versus iteration number for different number of events.
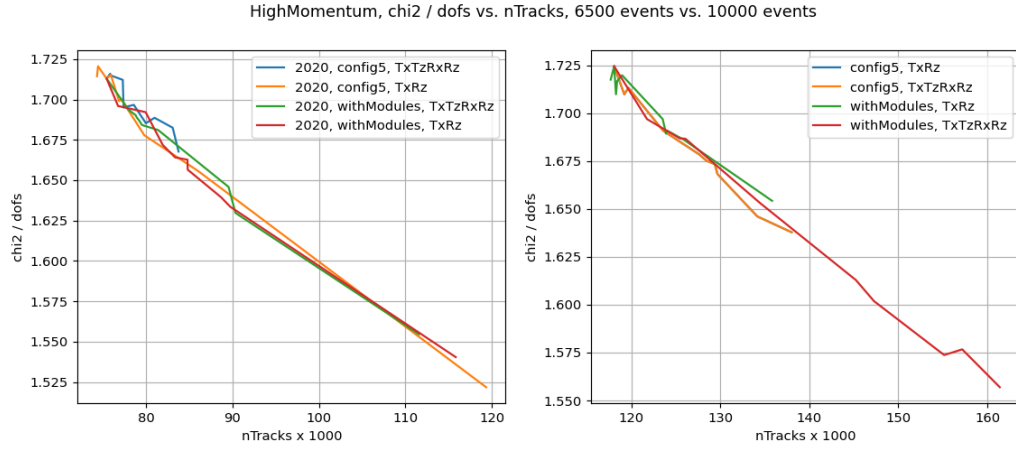
HighMomentum, chi2 / dofs vs. nTracks, 6500 events vs. 10000 events

Abbildung 4.17: $\chi^2/dofs$ versus number of Tracks for 6500 events and 10000 events.

4.5 luminosity samples and chi2

For a cross check regarding upcoming studies the difference in $\chi^2/dofs$ for samples of different luminosities are looked at. Comparing two samples, one with a "ramp-up" luminosity with a parameter $\nu = 3.8$ also referred to as "low luminosity" and one for the luminosity used during the data taking with $\nu = 7.6$, called "normal luminosity". The $\chi^2/dofs$ of these samples is plotted versus the iteration number 4.18 and the number of tracks4.19.

in figure 4.18 we see the expected convergence after iteration three and a quite low $\chi^2/dofs$ of around 1,285 95 for the normal luminosity sample and 1,3067 for the low luminosity sample.
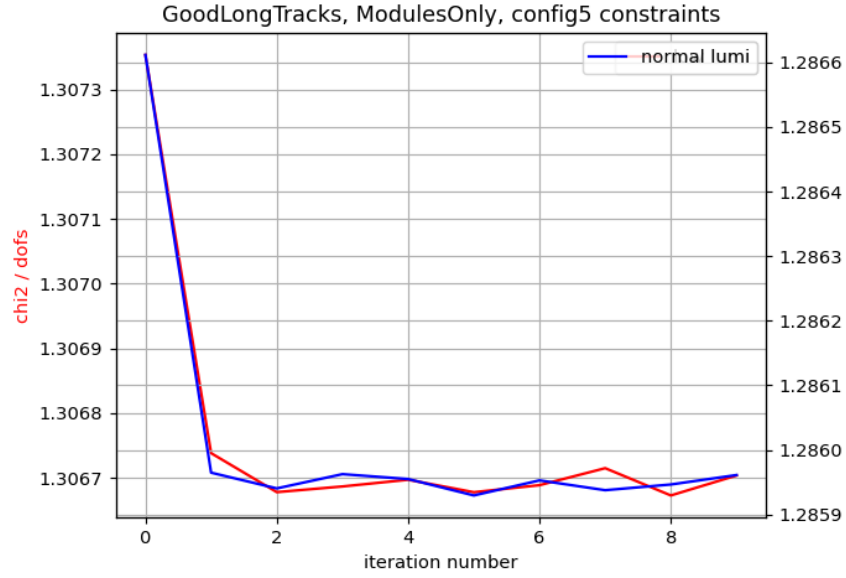
Abbildung 4.18: compare different luminosities and plot χ^2 versus iteration number.
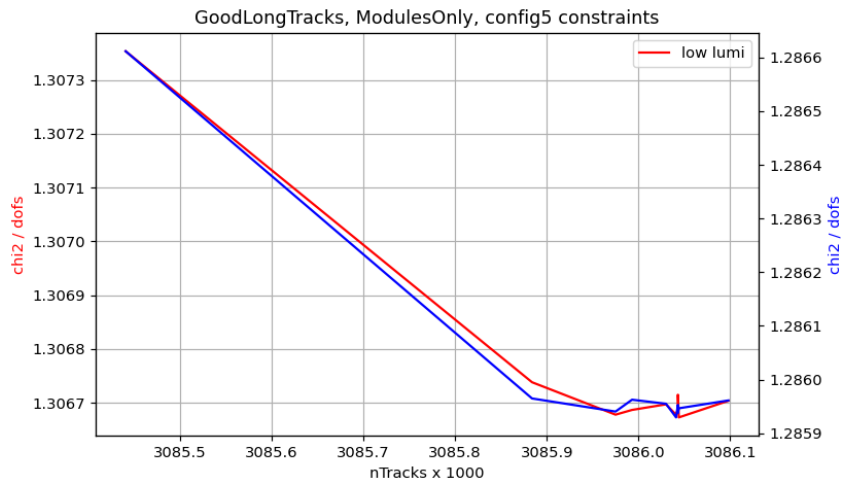

Abbildung 4.19: compare different luminosities and plot χ^2 versus number of tracks as a measurement for weakmodes and alignment.

4.6 impact of the cluster bias

As mentioned earlier the clusterbias most certainly causes the shift in the rotation around z for each layer so it does not reach 0. To test that a momentary fix was found and implemented. The workaround was to add a scaling for the *m_airgap*[11].

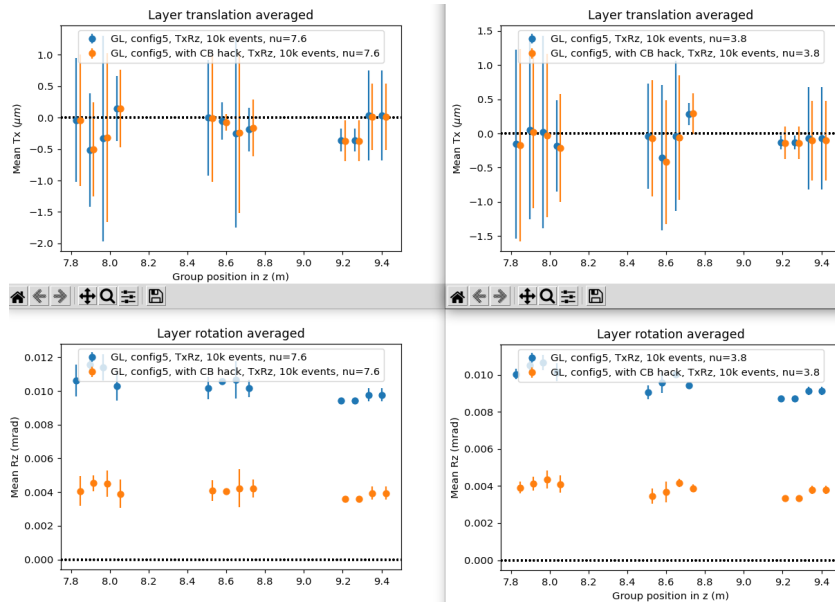Figure 4.20 shows the impact of the cluster bias fix regarding the rotation around z.

Abbildung 4.20: Impact of the clusterbias for high and low luminosity samples.

As we expected, the amount of rotation was reduced to about 0,004 mrad from the previous 0,01 mrad which is more than a factor of 2 improvement. We also know, that the fix for the cluster bias will not be the only source for the shift and we need further analysis to find the other sources.

Now that we know that the cluster bias can be taken care of we take a closer look at samples of different luminosities since the LHC will not be operated at the maximum luminosity from the start, there is also the ramp up phase where the luminosity will be lower.

Since we want to know what the shifts in rotation and translation will look like when the cluster bias is fixed we will keep it active for the next studies. Figure 4.21 shows the difference between a sample with ramp-up luminosity and a sample with the luminosity during the measurement phase. We see, that the layer separation is much

more prominent in station 1 and 3 for the higher luminosity sample but slightly better behaved in station 2 when looking at x-translation. Regarding the z-rotation, the lower luminosity sample as slightly lower rotational shifts. The difference is so minute that it can be safely disregarded. (not sure about that)

With that, we tested if there is a noticable difference in the $\frac{\chi^2}{\text{dof}}$ and the result is shown in figure 4.22.

Now, since the alignment works quite good with the current configuration we tested how translation misalignment effects the convergence by looking at the χ^2, portrayed in figure 4.23. For this figure, eight different samples of $100\,\mu\text{m}$ module translation misalignment over all translatory degrees of freedom. The idea behind using different samples is to reduce errors from biased samples. The plot shows the total χ^2 over degrees of freedom plotted against the number of iterations. We see no visible difference regarding the total χ^2 between the samples which is good. Also, the total χ^2 decreases with an increasing number of iterations during the alignment.

We do want the least amount of constraints in the system so we also tested the consequences of removing constraints from "config5". The results are shown in figure 4.24. The green curve shows the base configuration for comparison and in red the removal of the backlayer constraint in station 3 is shown. The blue curve shows the alignment results without the C-frame constraints. The data samples used were from 2020 with the normal luminosity and an active clusterbias fix. The selected track types are *HighMomentumTTracks* for 10000 events. On the one hand we see an improvement in χ^2/dof when removing these constraints individually even if it is only on a very small scale of $1 \cdot 10^{-5}$. On the other hand we see that the χ^2/dof after the last iteration is the same for the base config and for the blue measurement. The constraint removed in the red measurement seems to have the most impact from what was tested but the peak in iteration 6 has no logical explanation. Additional analysis regarding constraint removal will be done in the future to analyse this phenomenon further. Also the behavior of the not decreasing χ^2/dof requires more testing. What can be taken from this is that the removal of some constraints will help the alignment but the cause of some abnormalities require more testing.
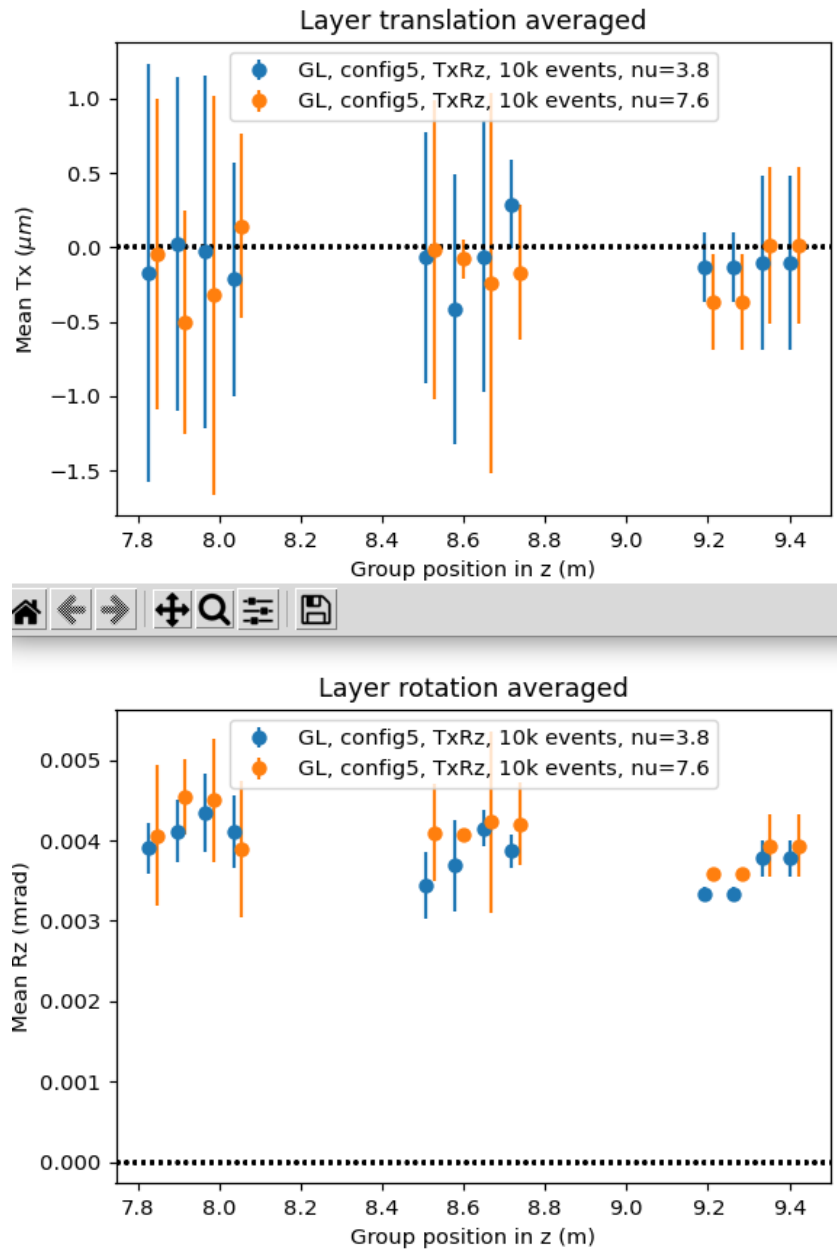
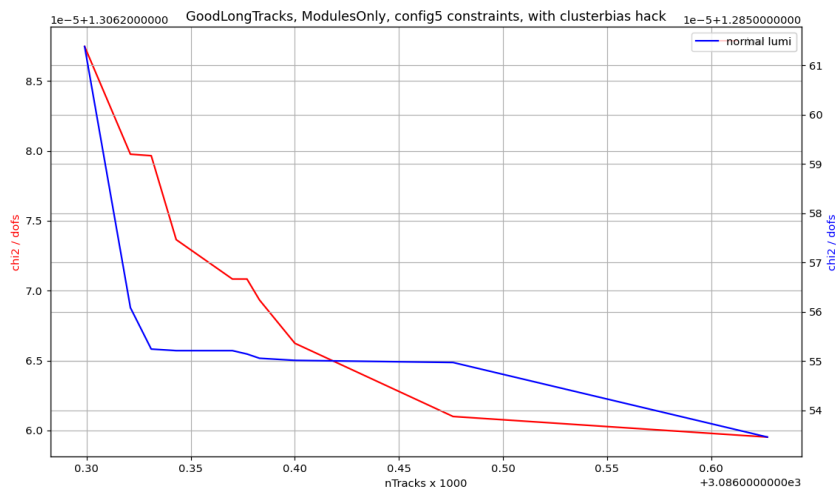**Abbildung 4.21:** show difference between low and normal luminosity with clusterbias fix active.

Abbildung 4.22: GoodLong tracks for module alignment and config 5 active. also the clusterbias fix is active comparing low and normal luminosity.
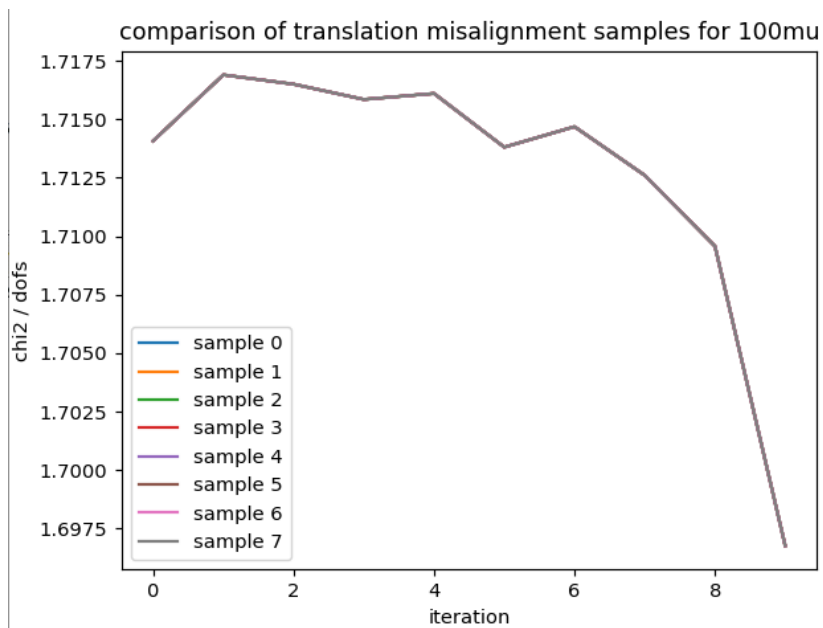

Abbildung 4.23: 100mu translation misalignment comparison for different misalignment samples.
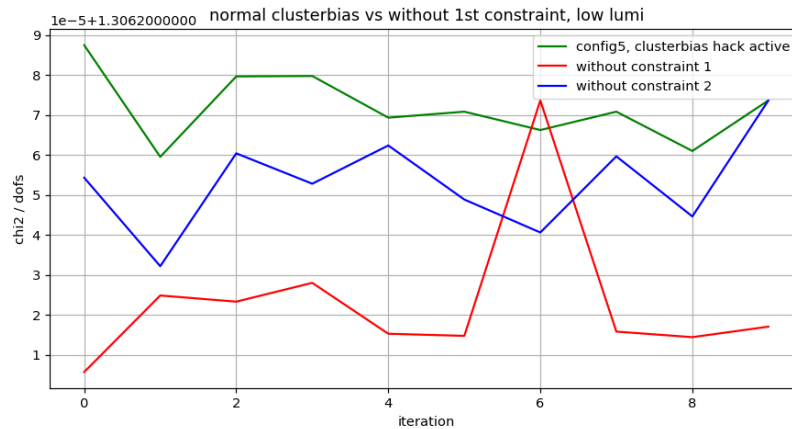
Abbildung 4.24: impact of removing constraints from exisiting studies regarding chi2.

4.7 Tests with input misalignments

In order to evaluate the performance of the alignment with a given configuration in Monte Carlo simulations, input misalignments are used.

5 Continuing Work

(Introduction part: - commissioning will continue for all of this year - moving from simulated studies to studies using data

Introduce the ways that your work is useful to commissioning:)

Input misalignments are a good way to retrieve information about how expected movements of the SciFi affect the alignment and monitoring outputs. When the data taking starts and and afterwards during times when the LHC is actively running, these simulated misalignment studies can be used for comparisons. One sign of a good alignment is the absence of the layer splitting. Similarly if the alignment is "good", in simulation it would converge towards the true aligned detector within three to five iterations. If the convergence happens later there is either a bias hindering the alignment or there is a problem with the configuration itself.

After the work in this thesis there are still more open questions for the SciFi alignment. The cluster bias which prevents the alignment from working correctly is currently being analysed, and when this is fixed the alignment will require more testing with simulation and data.

Additionally, there is another weak mode to consider in the SciFi, called the curvature bias. The curvature bias can appear in forward spectrometers with dipole magnets
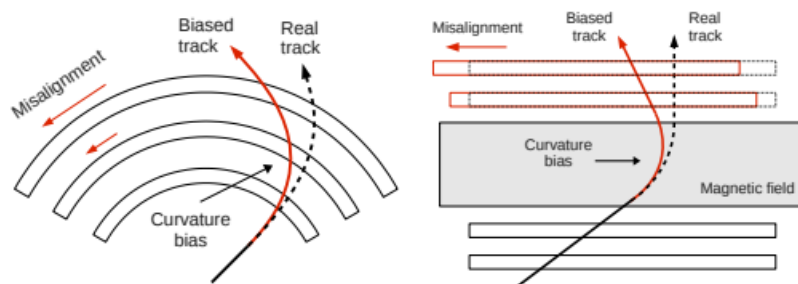

Abbildung 5.1: Illustration of a curvature bias in a central detector (left) and a forward detector (right).

like the LHCb experiment and cylindrical detectors with solenoidal magnetic fields as shown in figure 5.1. In forward spectrometers like LHCb, the curvature bias

can be caused by a superposition of relative shearing and rotation of the detectors surrounding the magnet. If a curvature bias is present, the reconstructed invariant mass of a two-body decay will be shifted proportionally to the momentum difference of the daughter particles in the final state[7]. There are two different ways to control the curvature bias. That is why alignment with particles will have an important role. Another way to constrain the curvature bias is to use magnet-off data, but this only works if the detectors do not move when the magnetic field is turned on. Recent commissioning measurements of LHCb show that the SciFi detector does move when the magnet turns on.

In order to perform a successful alignment for the SciFi Tracker the detectors upstream of the SciFi need to be installed and aligned as well. An essential part of the alignment is using correctly reconstructed long tracks, therefore the VELO has to be aligned to reconstruct good long tracks for the SciFi.

6 Conclusion

In order to handle increasing instantaneous luminosity and read out the data at 40 MHz, the LHCb has been upgraded. The new SciFi tracker is currently being commissioned, and the physics performance at LHCb will depend on how well the SciFi is aligned since poor alignment leads to systematic biases which can have a negative impact on sensitive asymmetry measurements. This thesis describes tests for the alignment using simulated data, which are used to find the best configuration for aligning the real detector and measure the expected accuracy of alignment.

Null tests were used to search for and correct for weak modes in the reconstruction software. A configuration called "config5 Rz", was found which gave the best results in this test. This constrains Tx, Tz and Rz in the last C-frame in station three. Only constraining station three in the given translational and rotational degrees of freedom improved the alignment for the first two stations regarding Tz.

Possible alignment configurations were also tested with input misalignment to the detector. After misaligning the modules in Tx, Ty and Tz for every layer in each station by 0,001 μm or by 200 μm, the system can return to its original alignment with differences that are small enough to be called negligible. The accuracy of the SciFi alignment to realistic translations is very good. On the other hand, it was found that misaligning the Modules in Rx, Ry and Rz for every layer in each station by 0,01 mrad resulted in misalignment of the SciFi detector that was difficult to correct with the alignment system, especially seen in Tz and Rz. The noticeable misalignment in Rz is also enlarged by the cluster bias effect. The cluster bias has a negative impact on Rz and increases the rotation around z by a factor of 2 compared to the simulation using a temporary fix for the bias. The true fix is currently being monitored and will improve the alignment once a solution is implemented.

Finally, the track selections for the alignment were also tested as part of the alignment configuration. The tests of the different track selections showed a strong correlation between the χ^2/dofs and the number of tracks. For the GoodLongTracks, including the additional alignment of the modules was found to improve the χ^2/dofs. The use of two translational and two rotational degrees of freedom compared to only Tx and Rz also improves the χ^2/dofs and the alignment.

Literatur

[1] *A diagram showing the complete structure of the LHC facility at CERN.* URL: https://www.researchgate.net/figure/A-diagram-showing-the-complete-structure-of-the-LHC-facility-at-CERN-There-are-the-4_fig8_348806406 (besucht am 09.03.2022).

[2] R. Aaij et al. „Analysis of Neutral B-Meson Decays into Two Muons“. In: *Phys. Rev. Lett.* 128.4 (2022), S. 041801. DOI: 10.1103/PhysRevLett.128.041801. arXiv: 2108.09284 [hep-ex].

[3] R. Aaij et al. „Precise determination of the B_s^0–$\overline{B}_s^0$ oscillation frequency“. In: *Nature Phys.* 18.1 (2022), S. 1–5. DOI: 10.1038/s41567-021-01394-x. arXiv: 2104.04421 [hep-ex].

[4] Roel Aaij et al. „Branching Fraction Measurements of the Rare $B_s^0 \to \phi\mu^+\mu^-$ and $B_s^0 \to f_2'(1525)\mu^+\mu^-$- Decays“. In: *Phys. Rev. Lett.* 127.15 (2021), S. 151801. DOI: 10.1103/PhysRevLett.127.151801. arXiv: 2105.14007 [hep-ex].

[5] Roel Aaij et al. „Measurement of the b-quark production cross-section in 7 and 13 TeV pp collisions“. In: *Phys. Rev. Lett.* 118.5 (2017), S. 052002. DOI: 10.1103/PhysRevLett.118.052002. arXiv: 1612.05140 [hep-ex].

[6] *Alignment.* URL: https://gitlab.cern.ch/lhcb/Alignment (besucht am 21.04.2022).

[7] J. Amoraal et al. „Application of vertex and mass constraints in track-based alignment“. In: *Nucl. Instrum. Meth. A* 712 (2013), S. 48–55. DOI: 10.1016/j.nima.2012.11.192. arXiv: 1207.4756 [physics.ins-det].

[8] Oliver Sim Brüning et al. *LHC Design Report.* CERN Yellow Reports: Monographs. Geneva: CERN, 2004. DOI: 10.5170/CERN-2004-003-V-1. URL: https://cds.cern.ch/record/782076.

[9] LHCb Collaboration. *LHCb Tracker Upgrade Technical Design Report.* Techn. Ber. Feb. 2014. URL: https://cds.cern.ch/record/1647400.

[10] CDF Collboration und T. Aaltonen et al. „High-precision measurement of the <i>W</i> boson mass with the CDF II detector“. In: *Science* 376.6589 (2022), S. 170–176. DOI: 10.1126/science.abk1781. eprint: https://www.science.org/doi/pdf/10.1126/science.abk1781. URL: https://www.science.org/doi/abs/10.1126/science.abk1781.

[11] *DeFTMat.cpp.* URL: `https://gitlab.cern.ch/lhcb/LHCb/-/blob/master/Det/FTDet/src/Lib/DeFTMat.cpp#63` (besucht am 03.05.2022).

[12] Christian Elsässer. *b̄b production angle plots.* URL: `%7B%5Chref%7Bhttps://lhcb.web.cern.ch/lhcb/speakersbureau/html/bb%5C_ProductionAngles.html%7D%7Bhttps://lhcb.web.cern.ch/lhcb/speakersbureau/html/bb%5C_ProductionAngles.html%7D%7D` (besucht am 06.05.2022).

[13] W.D. Hulsbergen. „The global covariance matrix of tracks fitted with a Kalman filter and an application in detector alignment". In: *Nuclear Instruments and Methods in Physics Research Section A: Accelerators, Spectrometers, Detectors and Associated Equipment* (2009), S. 471–477. DOI: `https://doi.org/10.1016/j.nima.2008.11.094`. URL: `https://www.sciencedirect.com/science/article/pii/S0168900208017567`.

[14] *LHC Machine.* URL: `https://cds.cern.ch/record/1129806/files/jinst8_08_s08001.pdf` (besucht am 09.03.2022).

[15] *LHCb Tracker Upgrade Technical Design Report.* URL: `https://cds.cern.ch/record/1647400/files/LHCB-TDR-015.pdf` (besucht am 09.03.2022).

[16] Rosen Matev. *testfileDB.py.* URL: `https://gitlab.cern.ch/lhcb-datapkg/PRConfig/blob/master/python/PRConfig/TestFileDB.py` (besucht am 20.03.2022).

[17] J Mazorra et al. „PACIFIC: the readout ASIC for the SciFi Tracker of the upgraded LHCb detector". In: *JINST* 11 (2016), S. C02021. DOI: `10.1088/1748-0221/11/02/C02021`. URL: `http://cds.cern.ch/record/2266414`.

[18] *Physical Constants.* URL: `http://pdg.lbl.gov/2019/mobile/reviews/pdf/rpp2018-rev-phys-constants-m.pdf` (besucht am 11.08.2019).

[19] Alessio Piucci. „The LHCb Upgrade". In: *Journal of Physics: Conference Series* 878 (Juli 2017), S. 012012. DOI: `10.1088/1742-6596/878/1/012012`. URL: `https://doi.org/10.1088/1742-6596/878/1/012012`.

[20] Alessio Piucci. „The LHCb Upgrade". In: *Journal of Physics: Conference Series* 878 (Juli 2017), S. 012012. DOI: `10.1088/1742-6596/878/1/012012`. URL: `https://doi.org/10.1088/1742-6596/878/1/012012`.

[21] *standard Model.* URL: `https://www.physik.uzh.ch/en/researcharea/lhcb/outreach/StandardModel.html` (besucht am 11.04.2022).

[22] *The invariant Rauch-Tung-Striebel Smoother.* URL: `http://ras.papercept.net/images/temp/IROS/files/2526.pdf` (besucht am 24.03.2022).

[23] *The LHCb Detector at the LHC.* URL: `https://cds.cern.ch/record/1129809/files/jinst8_08_s08005.pdf` (besucht am 09.03.2022).

[24] J Van Tilburg. „Track simulation and reconstruction in LHCb“. Presented on 01 Sep 2005. 2005. URL: https://cds.cern.ch/record/885750.

[25] T.O. White. „Scintillating fibres“. In: *Nuclear Instruments and Methods in Physics Research Section A: Accelerators, Spectrometers, Detectors and Associated Equipment* 273.2 (1988), S. 820–825. ISSN: 0168-9002. DOI: https://doi.org/10.1016/0168-9002(88)90102-7. URL: https://www.sciencedirect.com/science/article/pii/0168900288901027.

Danksagung

At this point i want to thank everyone who supported me during my time working on my master thesis.

I would like to say a huge thank you to Professor Spaan for allowing me to write my master's thesis at his department. At the same time, I would like to thank Professor Albrecht for standing in for Mr. Spaan and accompanying me the rest of the way.

I would also like to thank Dr. Weingarten for second-guessing my thesis.

Special thanks go to my supervisor Sophie Hollitt who taught me a lot about alignment and supported me during my time. My deepest thanks.

Thanks also to Lukas Calefice, Miroslav Saur for proofreading my work and Nicole Schulte for her support.

Finally, I would like to thank my family and close friends for supporting and motivating me throughout my journey.

Eidesstattliche Versicherung

Ich versichere hiermit an Eides statt, dass ich die vorliegende Abschlussarbeit mit dem Titel „Alignment studies for the LHCb SciFi Detector" selbstständig und ohne unzulässige fremde Hilfe erbracht habe. Ich habe keine anderen als die angegebenen Quellen und Hilfsmittel benutzt, sowie wörtliche und sinngemäße Zitate kenntlich gemacht. Die Arbeit hat in gleicher oder ähnlicher Form noch keiner Prüfungsbehörde vorgelegen.

_____   _____
Ort, Datum   Unterschrift

Belehrung

Wer vorsätzlich gegen eine die Täuschung über Prüfungsleistungen betreffende Regelung einer Hochschulprüfungsordnung verstößt, handelt ordnungswidrig. Die Ordnungswidrigkeit kann mit einer Geldbuße von bis zu 50 000,00 € geahndet werden. Zuständige Verwaltungsbehörde für die Verfolgung und Ahndung von Ordnungswidrigkeiten ist der Kanzler/die Kanzlerin der Technischen Universität Dortmund. Im Falle eines mehrfachen oder sonstigen schwerwiegenden Täuschungsversuches kann der Prüfling zudem exmatrikuliert werden (§ 63 Abs. 5 Hochschulgesetz –HG–).

Die Abgabe einer falschen Versicherung an Eides statt wird mit Freiheitsstrafe bis zu 3 Jahren oder mit Geldstrafe bestraft.

Die Technische Universität Dortmund wird ggf. elektronische Vergleichswerkzeuge (wie z. B. die Software „turnitin") zur Überprüfung von Ordnungswidrigkeiten in Prüfungsverfahren nutzen.

Die oben stehende Belehrung habe ich zur Kenntnis genommen.

_____   _____
Ort, Datum   Unterschrift